

RESEARCH

Open Access



# Polyzwitterion-branched polycholic acid nanocarriers based oral delivery insulin for long-term glucose and metabolic regulation in diabetes mellitus

Wenkai Zhang<sup>1,2,3,4</sup>, Yue Wang<sup>1,2,3,4</sup>, Xiangqi Zhang<sup>1,2,3,4</sup>, Yihui Zhang<sup>1,2,3,4</sup>, Wei Yu<sup>1,2,3,4</sup>, Haozheng Tang<sup>5</sup> and Wei-En Yuan<sup>1,2,3,4\*</sup>

## Abstract

Diabetes represents a global health crisis that necessitates advancements in prevention, treatment, and management. Beyond glucose regulation, addressing weight management and associated complications is imperative. This study introduces an oral nanoparticle formulation designed to simultaneously control blood glucose, obesity, and metabolic dysfunction. These nanoparticles, based on poly (zwitterion-cholic acid), incorporate a polyzwitterion component to enhance permeation through the mucus layer and prolong drug residence. Furthermore, bile acid polymers not only regulate lipid metabolism but also ameliorate obesity-associated inflammation in adipose and liver tissues. In vivo experiments demonstrated significant hypoglycemic effects in healthy, type I diabetic, and type II diabetic mice. Notably, the nanocarriers significantly reduced body weight gain, ameliorated inflammation in adipose and liver tissues, and modulated lipid metabolism in the liver of db/db mice. Our study elucidates a comprehensive strategy for addressing glycemic control and diabetes-related complications, offering a promising approach for diabetes prevention and treatment.

**Keywords** Oral delivery insulin, Zwitterionic nanoparticles, Obesity management, Diabetes, Metabolic regulation

\*Correspondence:

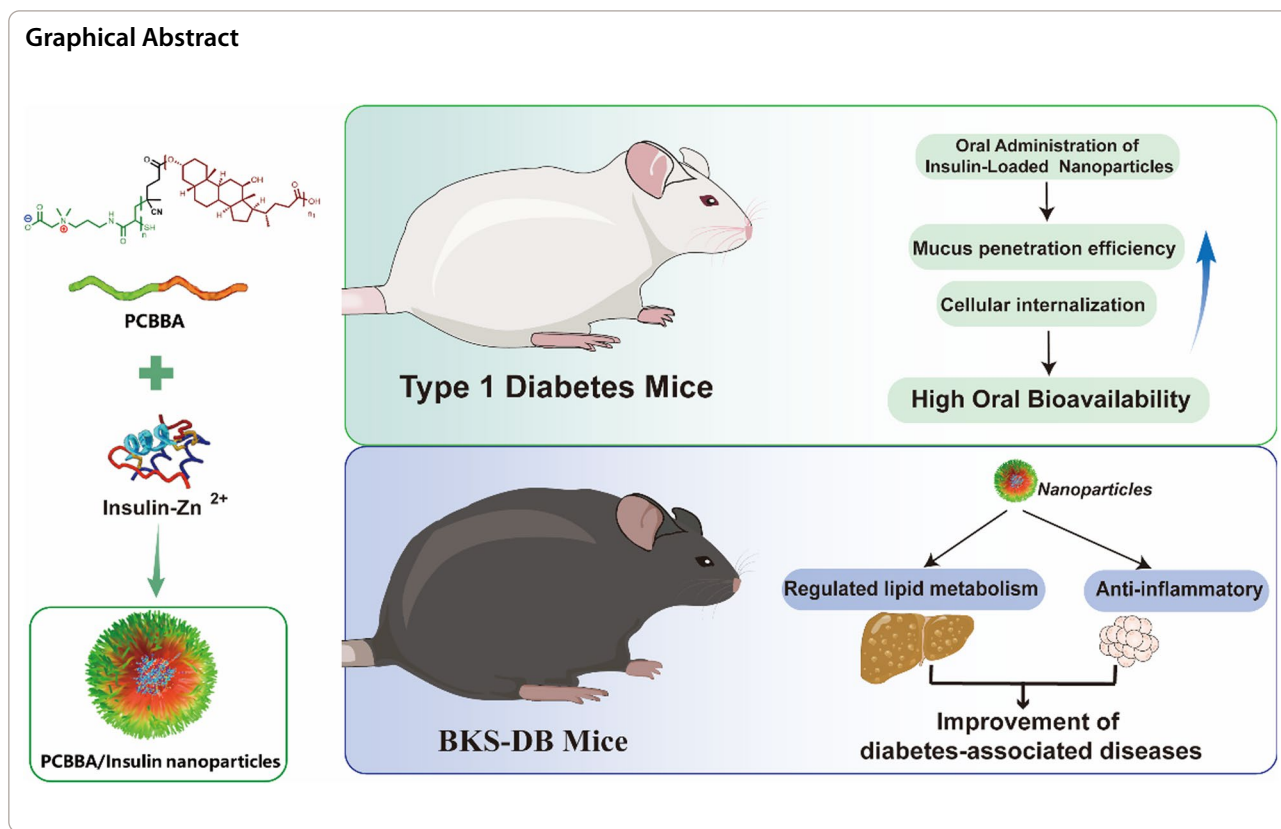
Wei-En Yuan

yuanweien@sjtu.edu.cn

Full list of author information is available at the end of the article



© The Author(s) 2025. **Open Access** This article is licensed under a Creative Commons Attribution-NonCommercial-NoDerivatives 4.0 International License, which permits any non-commercial use, sharing, distribution and reproduction in any medium or format, as long as you give appropriate credit to the original author(s) and the source, provide a link to the Creative Commons licence, and indicate if you modified the licensed material. You do not have permission under this licence to share adapted material derived from this article or parts of it. The images or other third party material in this article are included in the article's Creative Commons licence, unless indicated otherwise in a credit line to the material. If material is not included in the article's Creative Commons licence and your intended use is not permitted by statutory regulation or exceeds the permitted use, you will need to obtain permission directly from the copyright holder. To view a copy of this licence, visit <http://creativecommons.org/licenses/by-nc-nd/4.0/>.



## Introduction

Approximately one in ten adults worldwide currently live with diabetes, and this figure is anticipated to surpass 780 million within the next 25 years [1]. Therefore, finding more effective methods to prevent and treat diabetes, thereby enhancing the quality of life for diabetics, has become an imperative challenge [2, 3]. For individuals afflicted with diabetes, the primary goal is the management of blood glucose levels. Insulin, a cornerstone in diabetes management, is primarily administered through injections [4]. However, frequent injections can lead to discomfort and potential issues such as infection at the injection site. Consequently, achieving oral delivery of large-molecule drugs like insulin could significantly enhance patient well-being. Notably, there are no approved oral insulin products [5, 6]. The complexities surrounding the utilization of oral insulin formulations as a therapeutic approach for diabetes are manifold. Firstly, oral insulin demonstrates exceedingly low bioavailability, necessitating substantial doses to attain effective glycemic control [7, 8]. Secondly, the administration of high concentrations of insulin may exacerbate inflammatory responses and induce insulin resistance in patients [9]. Furthermore, insulin is limited to blood glucose regulation without conferring substantial improvements in

metabolic endocrine function or tolerogenic immunity in the longer term. Thus, diabetes treatment extends beyond glycemic control; it encompasses the management of complications, obesity, and inflammation in diabetic patients [4, 11, 12], highlighting the significance of a comprehensive approach to diabetes care.

To overcome the low oral bioavailability of insulin, researchers have developed various nanomaterials designed for the oral delivery of protein and peptide biomolecules. Nanoparticle platforms such as micelles, inorganic nanoparticles, and liposomes are widely employed for the oral administration of biomolecules [12–18]. However, most innovations in this field have primarily focused on optimizing insulin delivery efficacy while neglecting to address obesity, the pro-inflammatory response, insulin suppression, or metabolic dysfunction associated with diabetes. Consequently, there are no promising solutions that simultaneously address the inefficiency of oral insulin delivery and the metabolic issues related to diabetes mellitus.

Bile acids play a crucial role in solubilizing and facilitating the absorption of lipids and cholesterol in the intestine [19–21]. They are reabsorbed in the ileum and recirculated to the liver via the portal vein. Bile acids are involved in several key biological processes, including the regulation of glucose homeostasis, lipid metabolism, and

energy expenditure [22–27]. Structurally, bile acids are amphiphilic molecules consisting of a hydrophobic and rigid steroid backbone with hydrophilic hydroxyl groups [28–30]. Due to these properties, bile acids have potential applications not only in treating conditions such as diabetes and obesity but also as vehicles for the oral delivery of drugs. However, their low solubility in water limits their use as standalone oral delivery vehicles. Consequently, current research primarily focuses on modifying bile acids on the surface of nanoparticles to enhance the oral absorption of drugs [31–33]. In this study, we utilized bile acids as hydrophobic cores, aiming to leverage their beneficial effects on diabetes-related conditions. We propose modifying bile acids by covalently binding them with hydrophilic materials to create amphiphilic compounds that are more soluble in water, thereby enhancing their utility as drug-delivery vehicles for the oral administration of insulin and improving glucose and lipid metabolism in patients.

Zwitterionic materials have garnered significant attention in recent years due to their exceptional biocompatibility, superhydrophilicity, and antifouling properties [34–41]. These materials exhibit efficient mucus penetration and rapid transepithelial transport without disrupting the tight junctions of the intestinal epithelial cell layer, making them highly promising for oral drug delivery applications. Cao and co-workers [42] have shown that zwitterionic micelles can efficiently deliver oral insulin without opening tight junctions, Huang and co-workers [43] developed zwitterion functionalized nanoparticles loaded with insulin which could rapidly permeate the intestinal mucus layer and induce a prominent hypoglycemic response in diabetic rats following oral administration. Therefore, we plan to use zwitterionic materials to covalently bind to bile acids to form amphiphilic compounds and use these as carriers to prepare nanoparticles for oral delivery.

To address the multipronged challenges associated with the efficient oral delivery of insulin and amelioration or prevention of diseases such as obesity, metabolic dysfunction, and pro-inflammatory response during glycemic management, we synthesized an amphiphilic copolymer (PCBBA) comprised of polycarboxybetaine and polymeric ursodeoxycholic acid. Through the covalent conjugation of polymeric ursodeoxycholic acid with zwitterionic components, we have successfully synthesized amphiphilic PCBBA copolymers. These copolymers autonomously assemble into spherical nanoparticles in water, serving as carriers for insulin, thereby facilitating its oral administration. Within this micellar structure, polymeric ursodeoxycholic acid forms the hydrophobic core, while polycarboxybetaine forms the hydrophilic corona. We selected polymeric ursodeoxycholic acid for

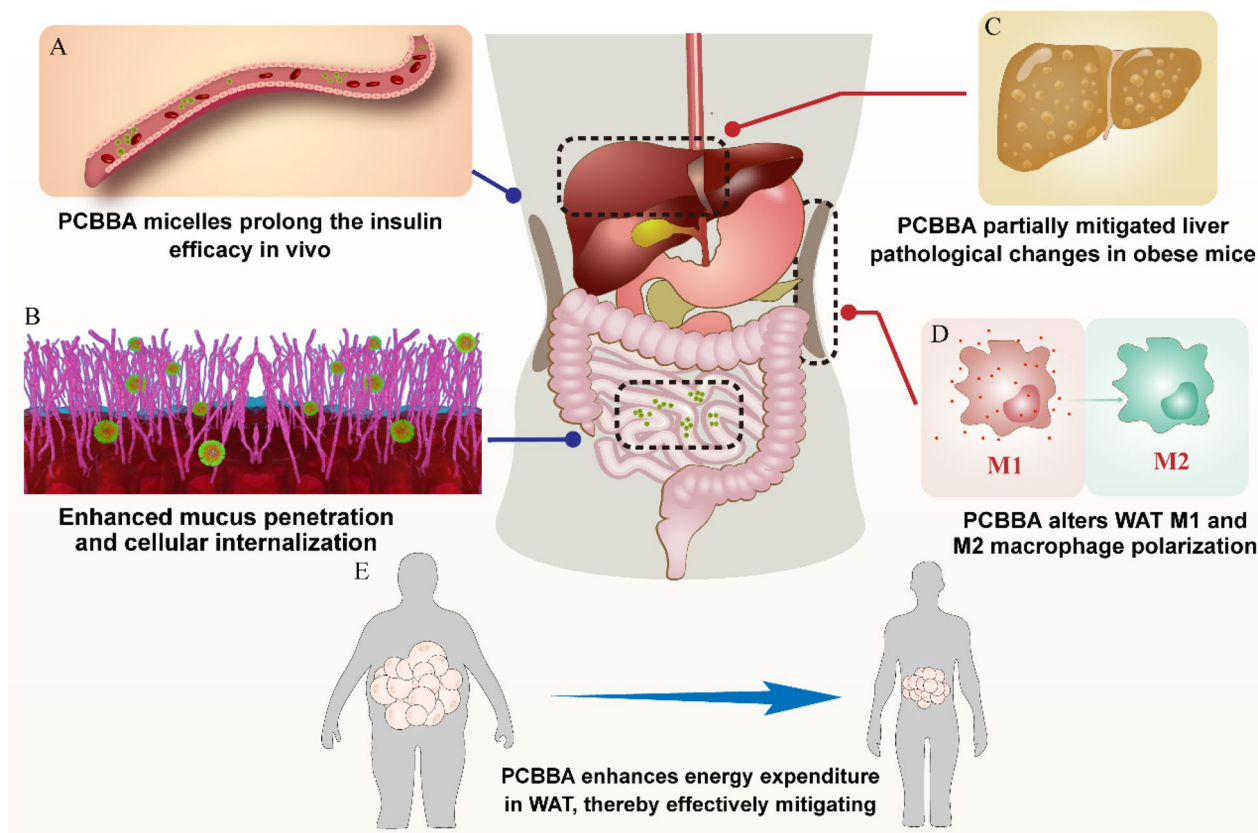
two primary reasons: (1) Bile acids, being amphiphilic molecules, when combined with hydrophilic polymers, can form an effective nanocarrier system [29, 44, 45]. (2) Polymeric ursodeoxycholic acid (PUDCA) exhibits high-avidity binding to the TGR5 receptor (Bile Acid-Responsive G Protein-Coupled Receptor) [46], potentially enhancing therapeutic outcomes such as anti-inflammatory responses and increased energy expenditure in adipose tissue. Polycarboxybetaine was chosen for its excellent biocompatibility, efficient mucus penetration, and rapid transepithelial transport without disrupting the tight junctions of the intestinal epithelial cell layer. Additionally, the polyzwitterion further stabilizes the micellar structure and prolongs the circulation time *in vivo* [35, 47–49].

In this research, PCBBA serves as a drug carrier, with the nanoparticles loaded with insulin efficiently penetrating the intestines and entering the bloodstream, thereby controlling blood glucose levels in diabetic mice. Moreover, this carrier has potential applications as a weight loss medication, fine-tuning lipid metabolism and energy expenditure, and ameliorating insulin resistance in diabetic patients. Together, this research represents progress in advancing the feasibility of oral insulin administration and offers novel avenues for the prevention and management of diabetes, obesity, and related disorders (Scheme. 1).

## Results and discussion

### Preparation and characterization of nanoparticles

The amphiphilic polymer PCBBA was synthesized and characterized as follows (Fig. S1–S7 Supporting Information). The polymer PCB was synthesized based on previous studies [50, 51]. Initially, the acrylamide-type monomer CB-tBu was synthesized (Fig. S1), followed by the preparation of PCB via reversible addition-fragmentation chain transfer (RAFT) polymerization. The  $^1\text{H}$  nuclear magnetic resonance (NMR) signal intensity provided information on the relative number of protons. The degree of polymerization was determined to be 22, based on the ratio of the proton peak areas at  $\delta_{\text{H}}$  0.89 and  $\delta_{\text{H}}$  4.53 in the  $^1\text{H}$  NMR spectra (Fig. S2). PCBBA was then obtained by esterifying the terminal carboxyl group of PCB with PUDCA. The cross-linking of PUDCA with PCB was demonstrated using gel permeation chromatography (GPC) to determine the number of average molecular weights, which were 1541 g/mol for PUDCA and 5019 g/mol for PCBBA (Figs. S5 and S6). Cross-linking was further confirmed by  $^1\text{H}$  NMR, distortionless enhancement by polarization transfer ( $^{13}\text{C}$ -DEPT 135), two-dimensional (2D) heteronuclear single-quantum coherence (HSQC) spectroscopy, and two-dimensional double-quantum-filtered correlation spectroscopy



**Scheme 1** Schematic representation of PCBBA for the treatment and prevention of diabetes

(DQF-COSY) (Fig. S4).  $^1\text{H}$  NMR spectra indicated that approximately 14.9% of PCB was modified by PUDCA. PEGBA was formed by covalently combining poly (ethylene glycol) of 5000 number average molecular weight with PUDCA. The chemical structure and molecular weight of the obtained polymer were confirmed by  $^1\text{H}$  NMR and GPC (Fig. S7).

Organic solvents can compromise the structural integrity of proteins and peptides. To avoid this, self-assembled PCBBA-ins nanoparticles were prepared by dissolving PCBBA and insulin in PBS (phosphate-buffered saline) (Fig. 1a). PEGBA-ins nanoparticles were prepared using the same method. The formation of an insulin/ $\text{Zn}^{2+}$  complex between insulin and zinc ions facilitated efficient encapsulation by both PCBBA and PEGBA through hydrophobic interactions. The encapsulation efficiencies, measured using a BCA assay, were  $92.0 \pm 3.5\%$  for PCBBA and  $90.5 \pm 3.7\%$  for PEGBA. In this document, “PCBBA nanoparticles” refers to unloaded PCBBA nanoparticles, while “PCBBA-ins nanoparticles” denotes insulin-loaded nanoparticles.

The critical micelle concentration (CMC) value is commonly used to describe the physical properties and stability of micelles [52, 53]. Pyrene was used as a probe in the

experiments; when micelles form in the aqueous phase, pyrene molecules preferentially locate inside or near the hydrophobic microdomains of the micelles, altering their photophysical properties compared to those in water. The change in fluorescence intensity was examined to determine the CMC value of the PCBBA micelles. The CMC value, defined as the concentration corresponding to the intersection of the tangent lines of the fluorescence intensity curves, was found to be 0.1 mg/mL (Fig. 1b). This lower CMC value compared to that of a low molecular weight surfactant like sodium dodecyl sulfate (CMC = 2.3 mg/mL) indicates that PCBBA micelles have better stability and are highly resistant to dissociation and dilution due to the large blood volume in the body.

Transmission electron microscopy (TEM) and dynamic light scattering (DLS) were used to examine the morphology of PCBBA nanoparticles. As shown in Figs. 1c and d, the nanoparticles were spherical with an average diameter of approximately 120 nm and were nearly neutral in charge (Fig. S8). Stability tests showed that neither the particle size nor the zeta potential changed significantly after 10 days of storage at room temperature. However, at 4 °C, particle size slightly decreased, potentially due to temperature-induced changes in CMC, although

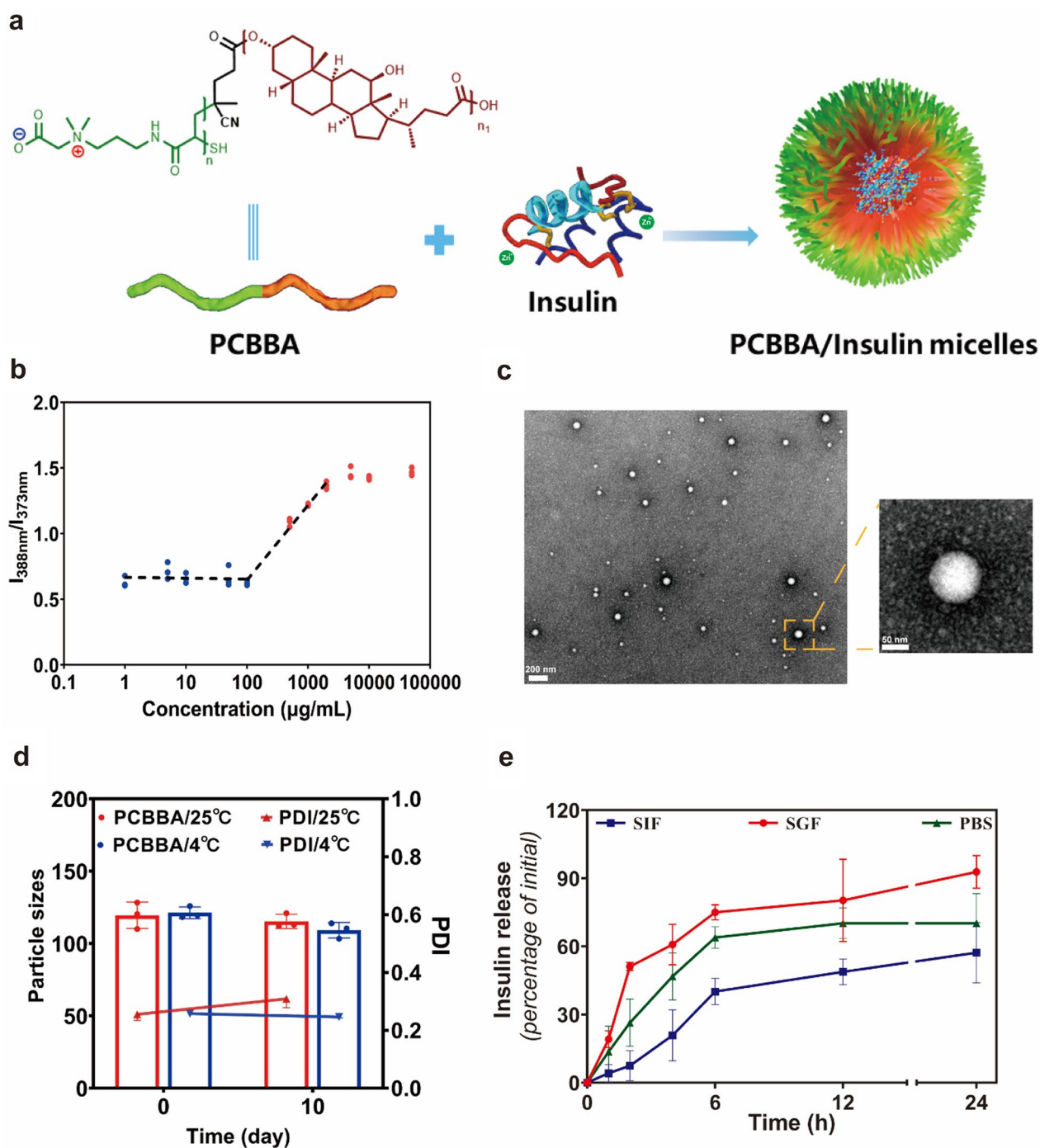


**Fig. 1** Preparation and characterization of the nanoparticles. **a** The chemical structure of PCBBA and the schematic illustration of its self-assembly with insulin into micelles. **b** Pyrene fluorescent emission intensity ratio ( $I_{388nm}/I_{373nm}$ ) was used to calculate the CMC of PCBBA micelles. **c** The TEM images of PCBBA nanoparticles (PCBBA micelles are approximately 100 nm in size. For simplicity, the term “PCBBA nanoparticles” will be used hereafter to refer to PCBBA micelles). **d** Particle size (left) and size distribution (PDI) of the nanoparticles after timed storage at room temperature or 4 °C. **e** Continuous release of insulin from PCBBA-ins under different environments. (n=3 independent samples, means ± SD)

this reduction was not statistically significant [54, 55] (Fig. 1d). These results indicate that the nanoparticles exhibit good stability, which is crucial for oral delivery.

The stability of drug-loaded nanoparticles in the gastrointestinal tract (GIT) is critical for the effective oral delivery of insulin. As shown in Fig. 1e, the nanoparticles

exhibited sustained-release properties, releasing less than 20% of the encapsulated insulin within one hour when exposed to simulated intestinal fluid (SIF). Insulin release was notably faster in simulated gastric fluid (SGF) compared to the other fluids, while release in SIF and PBS was slower, with SIF showing the slowest rate. Given the risk of rapid release of amphoteric micelles in gastric fluid, as observed in previous amphoteric ion studies [41, 42], we further assessed the stability of drug-loaded micelles in both SGF and SIF. The results indicated that free insulin was rapidly degraded in both fluids, whereas PCBBA-ins micelles provided some protection. However, due to the accelerated release of PCBBA-ins in SGF, only 40% of the active insulin remained after one hour of incubation (Figs. S9 and S10).

To address the instability of PCBBA-ins micelles in gastric fluid, we explored lyophilization followed by encapsulation into enteric capsules to preserve the integrity of the drug-loaded nanoparticles. The PCBBA-ins solution was first lyophilized, and the nanoparticles were re-dissolved in water to assess insulin activity using an ELISA (Enzyme-Linked Immunosorbent Assay). Additionally, oral administration of the same dose of nanoparticles to mice demonstrated that both pre- and post-freeze-dried PCBBA-ins nanoparticles exhibited comparable hypoglycemic effects (Fig. S18). These results indicate that the lyophilization process did not significantly affect insulin activity. Electron microscopy of the re-solubilized nanoparticles post-lyophilization showed no significant changes in morphology or particle size (Fig. S11). However, encapsulation efficiency slightly decreased to  $89.5 \pm 4.0\%$ , likely due to partial insulin leakage during the process. Despite this reduction, the nanoparticles remained stable enough to protect the insulin structure in the short term when placed in simulated intestinal fluid (SIF) (Fig. S10). In summary, PCBBA nanoparticles were successfully synthesized and characterized, demonstrating good stability and effective drug-carrying capacity. Although the nanoparticles exhibited rapid release in gastric fluid, they still provided short-term protection for insulin. Moreover, freeze-drying did not affect the structural integrity or activity of the insulin, and the re-solubilized nanoparticles retained particle size and morphology similar to the pre-lyophilized state. While the rapid release in gastric fluid poses a challenge, the freeze-drying process did not compromise the overall stability, making this a feasible strategy for oral delivery systems.

#### **PCBBA increases mucus penetration efficiency and cellular internalization**

For effective absorption, PCBBA nanoparticles must traverse the mucus layer that covers the surface of intestinal epithelial cells to reach the bloodstream [56–58]. In

our experimental setup, we simulated the mucus layer by applying a mucin solution onto Transwell inserts [59]. PCBBA/FITC-ins nanoparticles (loaded with FITC-insulin) were then applied on top of this simulated mucus layer, and their diffusion rate through the mucus was assessed by measuring the drug content in the basolateral chamber. Since UDCA (Ursodeoxycholic Acid) is not water-soluble, it cannot be directly used as a micellar carrier for insulin in oral delivery. To compare the oral delivery efficiency of PCBBA and evaluate its diffusion-promoting effects within the mucus layer, PEGBA was used as a control. PEG (polyethylene glycol), a commonly used hydrophilic material, can facilitate the oral delivery of nanoparticles; therefore, PEG-modified bile acids were employed to assess whether PCBBA could enhance nanoparticle diffusion through the mucus layer.

As shown in Figs. 2a and b, PCBBA nanoparticles exhibited significantly faster diffusion rates compared to PEGBA nanoparticles. Within four hours, PCBBA nanoparticles had nearly completely permeated into the basolateral chamber, demonstrating a diffusion rate 2–3 times higher than that of the control group. These results indicate that PCB-modified bile acids penetrate mucus more rapidly than PEG-modified bile acids, likely due to PCB's unique superhydrophilic and antifouling properties [39]. Consequently, PCB-modified bile acids can greatly enhance drug diffusion through the mucus layer. These findings highlight the rapid transit of PCBBA nanoparticles through the mucus layer, facilitating their subsequent uptake by intestinal epithelial cells.

A substantial body of research demonstrates that zwitterionic materials not only enhance micelle penetration in the mucus layer but also provide high transcellular transport efficiency without disrupting the tight junctions of the intestinal epithelium [41, 42, 61]. To evaluate cellular uptake, human colon adenocarcinoma (Caco-2) cells, which mimic the structure and function of small intestinal epithelial cells, were used as an *in vitro* model. Caco-2 cells were incubated with PCBBA-FITC-ins nanoparticles, and confocal laser scanning microscopy (CLSM) was used to visualize nanoparticle distribution within the cells. As shown in Fig. 2c, the PCBBA/FITC-ins group displayed a stronger fluorescent signal, indicating more efficient cellular uptake of the PCBBA nanoparticles.

Given that the intestinal epithelial layer poses the greatest challenge to the oral absorption of nanocarriers, previous *in vitro* experiments demonstrated that PCBBA nanoparticles could rapidly cross the mucus layer on the intestinal surface and were quickly taken up by Caco-2 cells. To further validate the stability, mucus permeation, and cellular uptake of PCBBA nanoparticles, we examined their transit ability in the mouse intestine.

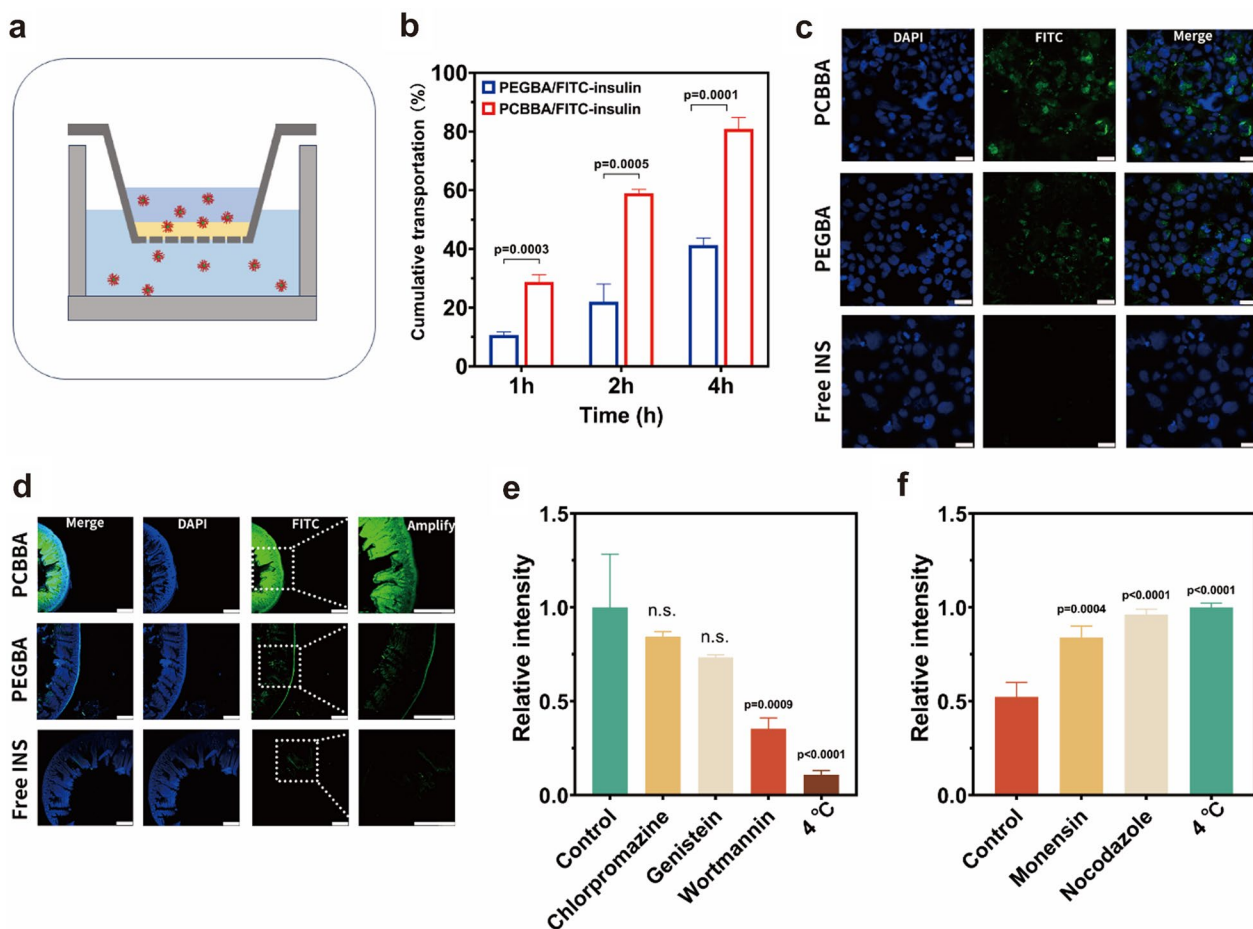


**Fig. 2** Mucus penetration, in situ absorption, and in vitro transcellular transport of PCBBA nanoparticles. **a** The schematic illustration of the transwell model, PCBBA-FITC-Ins nanoparticles pass through a simulated intestinal mucus layer deposited on a transwell membrane. At predetermined time intervals, the solution from the basolateral chamber is collected to detect fluorescence intensity. **b** Cumulative transportation of FITC-insulin from different nanoparticles at the predetermined time. **c** Cellular uptake of different nanoparticles into Caco-2 cells observed by confocal microscopy (scale bars, 20  $\mu$ m). **d** CLSM images of sectioned intestine tissues of diabetic mice after oral administration of different FITC-insulin formulations for 2 h. (n = 3 biologically independent samples, means  $\pm$  SD. Scale bars, 250  $\mu$ m). **e** Endocytosis pathway analysis. Caco-2 cells were pre-incubated with different endocytosis inhibitors for 2 h, incubated with PCBBA-FITC-insulin nanoparticles for 1 h, and then isolated for flow cytometry analysis. **f** Caco-2 cells were incubated with PCBBA-FITC-insulin nanoparticles for 3 h, washed and incubated with different inhibitors for 6 h, and then isolated for flow cytometry analysis

Drug-loaded nanoparticles were administered orally to mice, after which their intestines were excised, frozen sections were prepared, and CLSM was used to observe nanoparticle distribution. As shown in Fig. 2d, PCBBA/FITC-ins nanoparticles exhibited strong fluorescence on the microvillus surface and in the basolateral tissue of the small intestine, with higher fluorescence intensity compared to other groups. These results are consistent with earlier findings, Amphoteric ions have fast mucus shuttling ability due to their special hydrophilic and anti-fouling properties. Additionally, amphoteric ions demonstrate high efficiency in transcellular transport. Consequently, these experiments suggest that PCBBA shares similar properties with previously reported

polyzwitterionic nanoparticles, specifically regarding their ability to rapidly traverse the mucus layer and the small intestinal epithelial cells. Therefore, PCBBA nanoparticles hold significant potential for the oral delivery of drugs.

**Trans epithelial transport and mechanism of nanoparticles**

To investigate the transcellular transport mechanisms of PCBBA nanoparticles, we analyzed the endocytosis and exocytosis of PCBBA-FITC-ins nanoparticles in Caco-2 cells using flow cytometry. To elucidate the mechanisms underlying micelle uptake, several key components of endocytic pathways were blocked using common endocytosis inhibitors [60–62]. Figure 2e illustrates the impact

of these inhibitors on the cellular uptake of PCBBA-FITC-ins nanoparticles. Among them, the endocytosis of the PCBBA nanoparticles was most significantly suppressed at low temperatures (89.1%). Temperature substantially influences ligand-receptor interactions and the biological activity of numerous membrane proteins, making it an indicator of energy-dependence. This suggests that PCBBA nanoparticles entered into Caco-2 cells via an energy-dependent pathway. Additionally, genistein (26.6%) and wortmannin (64.7%) also suppressed micelle internalization, suggesting that PCBBA nanoparticles primarily enter cells via macropinocytosis and the lipid raft/caveolae pathway.

To explore the exocytosis mechanisms of PCBBA nanoparticles, we introduced a Golgi-related inhibitor (monensin, MON) and a microtubule pathway inhibitor (nocodazole, NO). As shown in Fig. 2f, both pathways were involved in the exocytosis of PCBBA nanoparticles. Additionally, a reduction in temperature markedly decelerated the exocytosis process, providing further evidence for the involvement of energy-dependent pathways in the exocytosis of PCBBA nanoparticles.

#### **In vivo biodistribution and intestine absorption**

The absorption rate of nanoparticles in the intestine and their in vivo distribution were assessed using the Maestro in vivo imaging system and confocal laser scanning microscopy (CLSM). Two types of PCBBA nanoparticles loaded with different fluorescent dyes were prepared: PCBBA-DIR nanoparticles (loaded with DiR iodide) and PCBBA-FITC-ins nanoparticles (loaded with FITC-insulin) [63]. Before the experiment, animals were fasted overnight and then administered PCBBA-DIR nanoparticles, PEGBA-DIR nanoparticles, or free DIR via oral gavage. Two hours post-gavage, mice treated with PCBBA-DIR showed a pronounced fluorescence signal, significantly stronger than that observed in the free DIR and PEGBA-DIR groups (Fig. 3a and b), suggesting that PCBBA nanoparticles are more rapidly enriched and absorbed in the intestinal tract.

To further investigate the absorption and biodistribution of the nanoparticles, parallel studies were conducted using a different dye (FITC). Similar results were observed when mice were orally administered nanoparticles loaded with FITC-insulin. Based on the intensity of the fluorescent signal from FITC-insulin in the intestines and major organs, it was further demonstrated that PCBBA nanoparticles rapidly accumulate and are absorbed in the intestines (Fig. 3d and e). Notably, strong fluorescence signals were detected in the liver, indicating that PCBBA nanoparticles likely circulate initially through the portal veins to the liver

(Fig. 3c). Additionally, prominent fluorescence signals were observed in the gall bladder, suggesting a potential involvement of enterohepatic circulation in the transport mechanism. In conclusion, these in vivo and in vitro experiments further demonstrate that PCB-modified bile acid nanoparticles can rapidly traverse the mucus layer of intestinal epithelial cells and enter systemic circulation.

#### **In vivo pharmacodynamics and pharmacokinetics studies**

To evaluate the efficacy of orally administered PCBBA-insulin compared to the standard subcutaneous insulin injection, we administered PEGBA-insulin (30 IU/kg), PCBBA-insulin (30 IU/kg), and free insulin (30 IU/kg) via gavage to streptozotocin (STZ)-induced diabetic Balb/c mice. For the control group, free insulin (5 IU/kg) was administered subcutaneously to STZ-induced diabetic Balb/c mice. Blood glucose levels were monitored using a glucometer (Fig. 4a). Results showed that the control group receiving subcutaneous insulin experienced a rapid decrease in blood glucose levels within 2 h, with the hypoglycemic effect diminishing after 5 h. In contrast, PCBBA-insulin significantly reduced blood glucose levels within the first 4 h and maintained this reduction for over 10 h, outperforming PEGBA-insulin (Fig. 4b). Oral administration of varying doses of PCBBA-insulin to diabetic mice resulted in different levels of blood glucose reduction, demonstrating the dose-dependency of PCBBA-insulin nanoparticles (Fig. 4c). Conversely, oral administration of free insulin or PCBBA alone did not lead to significant changes in blood glucose levels. Further evaluation in healthy mice and db/db mice (a type 2 diabetes model) confirmed that PCBBA significantly enhanced the oral bioavailability of insulin (Fig. 4d and e). Overall, the PCBBA-insulin formulation exhibited an effective hypoglycemic effect when administered orally. These experiments further demonstrated that PCBBA improved the oral delivery efficiency of insulin in vivo, with the PCB-modified carrier displaying superior oral delivery efficiency. This finding is consistent with previous in vitro results, highlighting PCBBA's high potential for oral drug delivery.

Since calculating oral relative bioavailability based on time-glucose curves can be affected by multiple factors, we conducted an additional experiment to directly measure serum insulin levels after oral administration of PCBBA-insulin. Using a human insulin ELISA kit, serum insulin concentrations were assessed, with subcutaneous insulin injection and oral free insulin as controls. Based on the area under the curve (AUC<sub>0-12 h</sub>) of serum insulin levels, the relative bioavailability of orally administered PCBBA-insulin was calculated to be 23.7% (Fig. 4f).

Further pharmacokinetic studies were conducted in Sprague Dawley (SD) rats to assess the oral

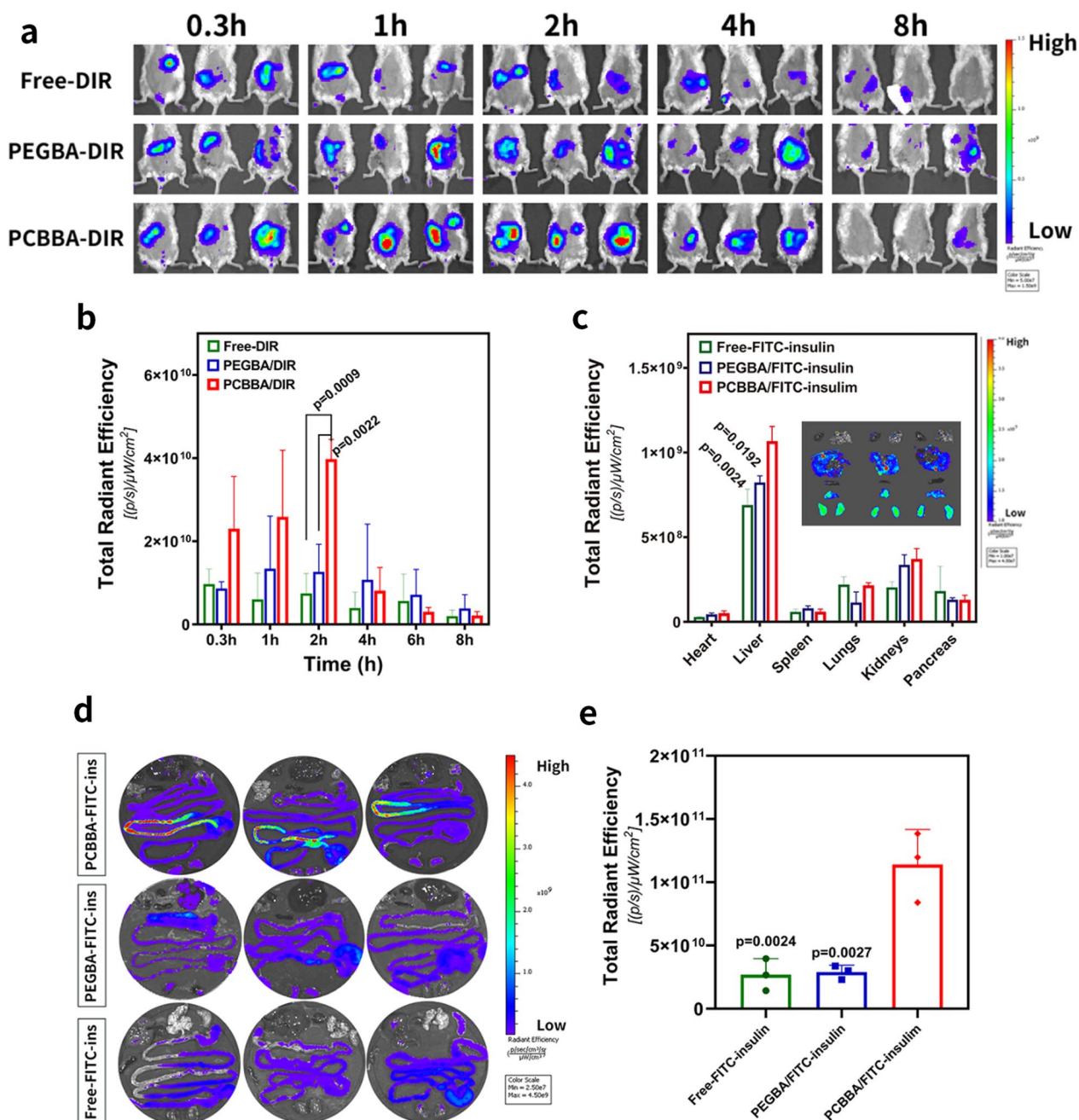


**Fig. 3** The in vivo biodistribution and intestine absorption of nanoparticles following the oral administration. **a** Fluorescence distribution and intensity of the DIR in vivo after timed intervals of oral administration of different formulations. **b** Quantification of the fluorescence intensity in vivo from panel (a). **c** Quantification of the fluorescence intensity of heart, liver, spleen, lungs, kidneys, and intestine from panel (d) and ex vivo fluorescence imaging of major organs after the oral PCBBA/FITC-ins administration for 2 h (insets). **d, e** Ex vivo fluorescence imaging of the heart, liver, spleen, lungs, kidneys, and intestine of the mice after the oral administration for 2 h and quantification of overall fluorescence intensity (e). All fluorescence intensities were quantified with Living Image® (n = 3 biologically independent animals, means ± SD)

bioavailability of PCBBA-insulin. Previous studies indicated that PCBBA nanoparticles are released more rapidly under acidic conditions, potentially reducing insulin bioavailability. To address this, we lyophilized

PCBBA-insulin nanoparticles, encapsulated them in enteric-coated capsules, and administered them via gavage. Blood samples were collected at different time points, and serum insulin levels were measured using a

human insulin ELISA kit (Fig. 4g). Serum insulin concentrations peaked at 12 h and remained elevated for an extended period. This prolonged effect is likely due to the delayed release of PCBBA-insulin in the intestines, facilitated by the enteric coating, which slowed the onset of action but extended circulation time. Based on the area under the curve (AUC<sub>0-48 h</sub>) of serum insulin concentrations, the relative bioavailability of insulin after oral administration of PCBBA-insulin capsules was approximately 32.9%. These results suggest that encapsulating PCBBA-insulin in enteric-coated capsules mitigates rapid release in gastric fluid and enhances oral insulin bioavailability, effectively delivering insulin to the bloodstream and extending its hypoglycemic action.

#### PCBBA as a potential anti-obesity agent

Cholic acid was selected for this study due to its potential to alleviate diabetes-related complications, such as obesity. To validate this hypothesis, we further evaluated the role of PCBBA in db/db mice. Polymeric ursodeoxycholic acid (PUDCA) was used as a control to compare PCBBA's effects. The db/db mouse model, which mimics type II diabetes, is characterized by elevated blood glucose levels and weight gain. To explore the impact of PCBBA on metabolic disorders like obesity, inflammation, and fatty liver, we administered PCBBA nanoparticles to db/db mice every three days over two weeks. We then measured body weight, fat mass, and adipose-related gene expression (Fig. 5). Mice treated with PCBBA showed a reduction in body weight to 83.6% of the control group, with similar effects observed in the PUDCA-treated group. Further analysis revealed that the weight reduction was primarily due to a decrease in white adipose tissue (WAT) mass, with the WAT-to-body-weight ratio also decreasing (Fig. 5a–c). These results suggest that PCBBA effectively reduces body weight in db/db mice, comparable to PUDCA's effects.

We hypothesized that the weight loss effect of PCBBA was primarily driven by its bile acid content. To explore the underlying mechanisms further, we focused on the potential role of bile acids in weight regulation. Although

monomeric UDCA may not be the most potent activator of TGR5, bile acid polymers, such as PCBBA, exhibit a higher affinity for the TGR5 receptor [64, 65]. Activation of TGR5 can induce significant weight loss in obese mice by initiating a thermogenic response in both brown adipose tissue (BAT) and white adipose tissue (WAT). This process counteracts diet-induced obesity and induces WAT browning [66–69]. To investigate whether the weight loss induced by PCBBA was associated with the browning of WAT, we analyzed the mRNA levels of several browning markers. Both PCBBA and PUDCA upregulated the expression of multiple genes associated with WAT browning, including uncoupling protein-1 (Ucp-1), when compared to the control group (Fig. 5d–f). This gene upregulation stimulates mitochondrial uncoupling and energy expenditure, effectively mitigating obesity in db/db mice [70–74]. Furthermore, WAT adipocytes in the PCBBA-treated group were significantly smaller (Fig. 5g), indicating a reduction in lipid accumulation. Overall, these findings demonstrate that PCBBA effectively promotes WAT browning and reduces obesity in db/db mice, with effects comparable to PUDCA.

#### PCBBA potentially ameliorates adipose inflammation, poor glucose tolerance, and insulin resistance in db/db mice

We conducted both an oral glucose tolerance test (OGTT) and an intraperitoneal insulin tolerance test (IPITT) to assess the effects of PCBBA and PUDCA on insulin sensitivity in obese mice. The results clearly demonstrated that both PCBBA and PUDCA significantly enhanced insulin sensitivity (Fig. 6a–d). Notably, the benefits of bile acid polymers, such as PCBBA and PUDCA, in diabetic mice extended beyond weight loss to include improvements in diabetes-related complications. These improvements can be attributed to the activation of the TGR5 receptor. TGR5 activation raises cyclic adenosine monophosphate (cAMP) levels, which in turn activates protein kinase A. This activation promotes the phosphorylation of target proteins, including the cAMP response element-binding protein (CREBP) transcription factor [25]. As a result, TGR5 activation not only increases

(See figure on next page.)

**Fig. 4** Pharmacodynamics and bioavailability of oral PCBBA nanoparticles. **a** Experimental scheme: Establish an STZ-induced diabetic mice model. **b,c** The blood glucose level of initial versus time profiles of the (STZ)-induced Balb/c diabetic mice following the oral administration of different nanoparticles loaded with insulin (**b**) and PCBBA drug-laden nanoparticles in different doses (10 IU/kg and 20 IU/kg) (**c**). Subcutaneously (s.c.) injected native insulin at 5 IU/kg was used as a control. (n = 6 biologically independent animals, means ± SD). **d** Blood glucose-lowering performance of the PCBBA/insulin nanoparticles on healthy mice through oral gavage. **e** Blood glucose-lowering performance of the PCBBA/insulin nanoparticles on db/db diabetic mice through oral gavage. (n = 3 biologically independent animals, means ± SD). **f** The serum insulin concentration (bioavailability) for the PCBBA/insulin nanoparticles on healthy mice through oral gavage and subcutaneously injected native insulin at 3 IU/kg was used as a control. (n = 6 biologically independent animals, means ± SD). **g** The serum insulin concentration (bioavailability) for the PCBBA/insulin capsules on healthy rats through oral gavage and subcutaneously injected native insulin at 5 IU/kg was used as a control. (n = 6 biologically independent animals, means ± SD)

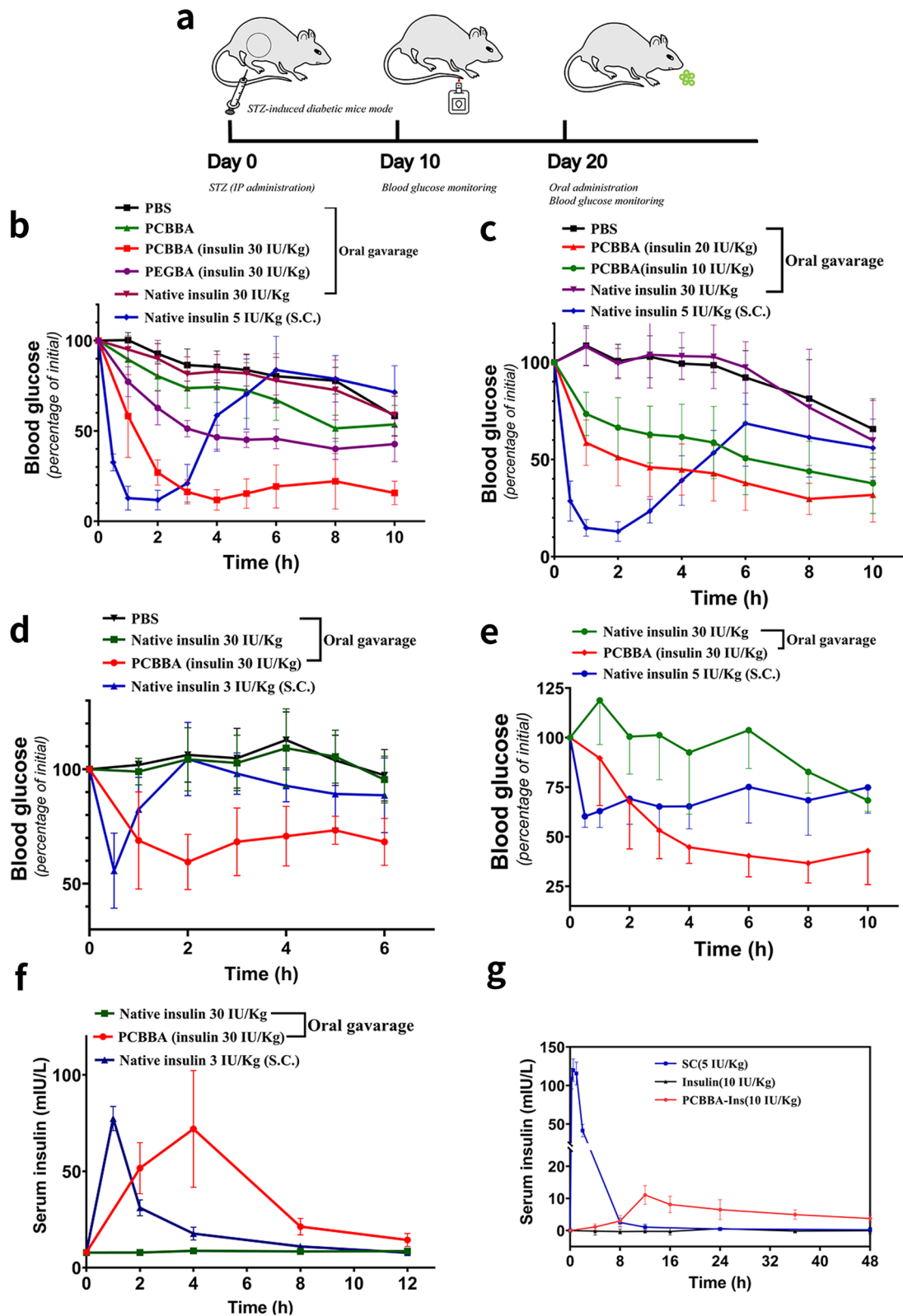
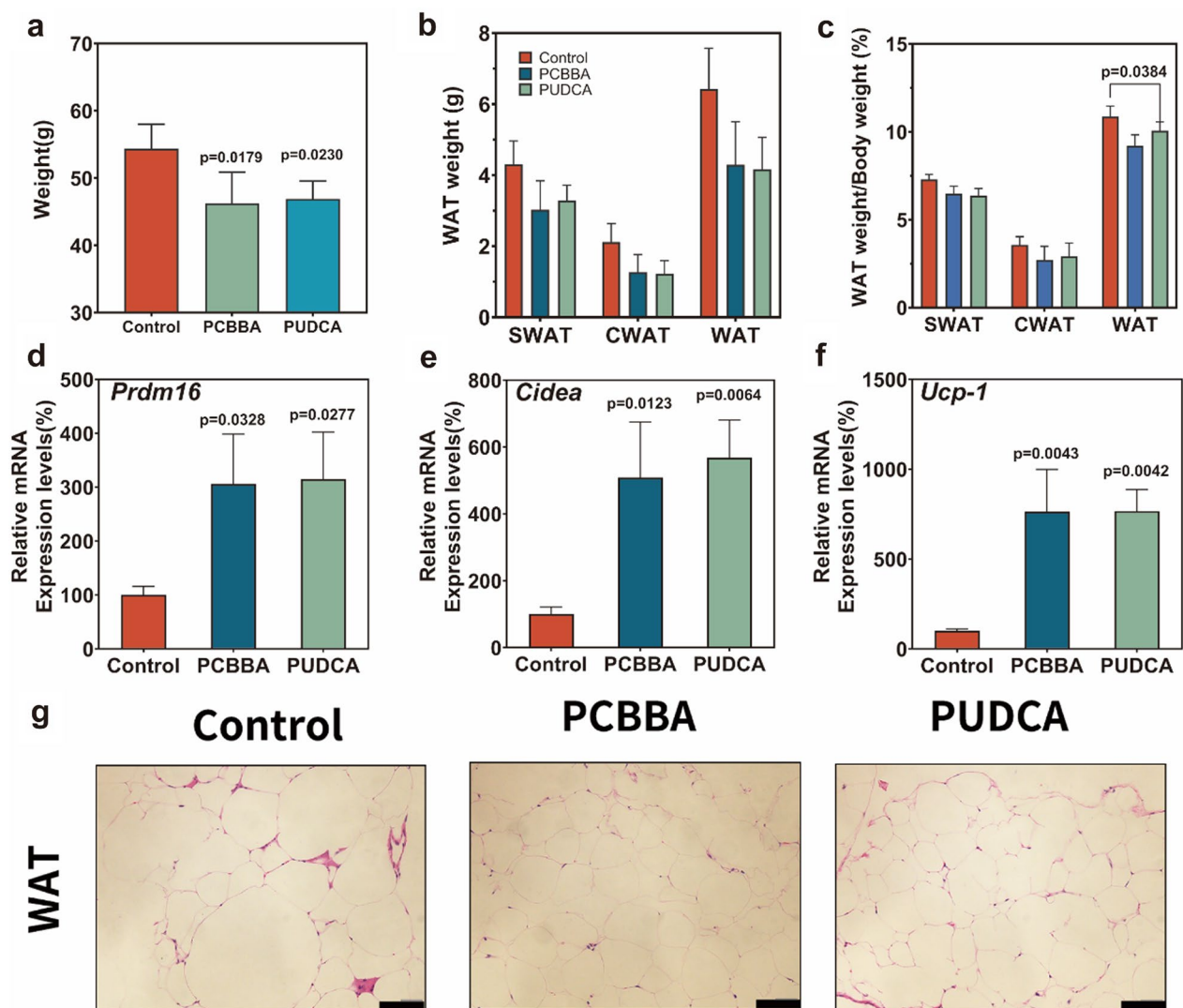


Fig. 4 (See legend on previous page.)



**Fig. 5** PCBBA Reduces Adiposity and Induces Browning of WAT in db/db Mice. **a** Body weight, **b** WAT weight, and **c** the ratio of WAT weight to body weight of db/db mice after oral administration every three days for two weeks. **d–f** The mRNA levels of brown adipocyte markers in WAT were determined by quantitative real-time PCR analysis. **g** Representative hematoxylin and eosin (H&E) staining of the WAT. (n=3 biologically independent samples, means  $\pm$  SD, Scale bar: 100  $\mu$ m.)

energy expenditure in adipose tissue but also enhances glucose metabolism and insulin sensitivity, while regulating the anti-inflammatory responses of macrophages [24, 75–77]. To further evaluate PCBBA's effects, we explored the potential underlying mechanisms in greater detail.

Adipose inflammation and aberrant production of adipokines/cytokines are key mediators linking obesity and its metabolic complications. Reversing these obesity-induced pathological abnormalities in white adipose tissue (WAT) may be crucial for improving glucose intolerance and insulin resistance in obese mice. In this study, we analyzed the gene expression of two inflammatory cytokines (TNF- $\alpha$  and IL-1 $\beta$ ) in WAT of obese

mice using real-time fluorescence quantitative PCR and observed a reduction in these inflammatory factors (Fig. 6f and g). Furthermore, the accumulation of macrophages in adipose tissue and a shift to an M1-like macrophage polarization state are major contributors to insulin resistance [78–80]. As illustrated in Fig. 6e, we used immunofluorescence microscopy to identify distinct subsets of adipose tissue macrophages (ATMs) based on the markers F4/80 $^{+}$ , CD11c $^{+}$ , and CD206 $^{+}$ . PCBBA significantly reduced the number of macrophages in adipose tissue, decreased M1 markers (F4/80 $^{+}$  CD11c $^{+}$ ), increased M2 markers (F4/80 $^{+}$  CD206 $^{+}$ ), and improved the ratio of M1 to M2 ATMs in db/db mice. The activated

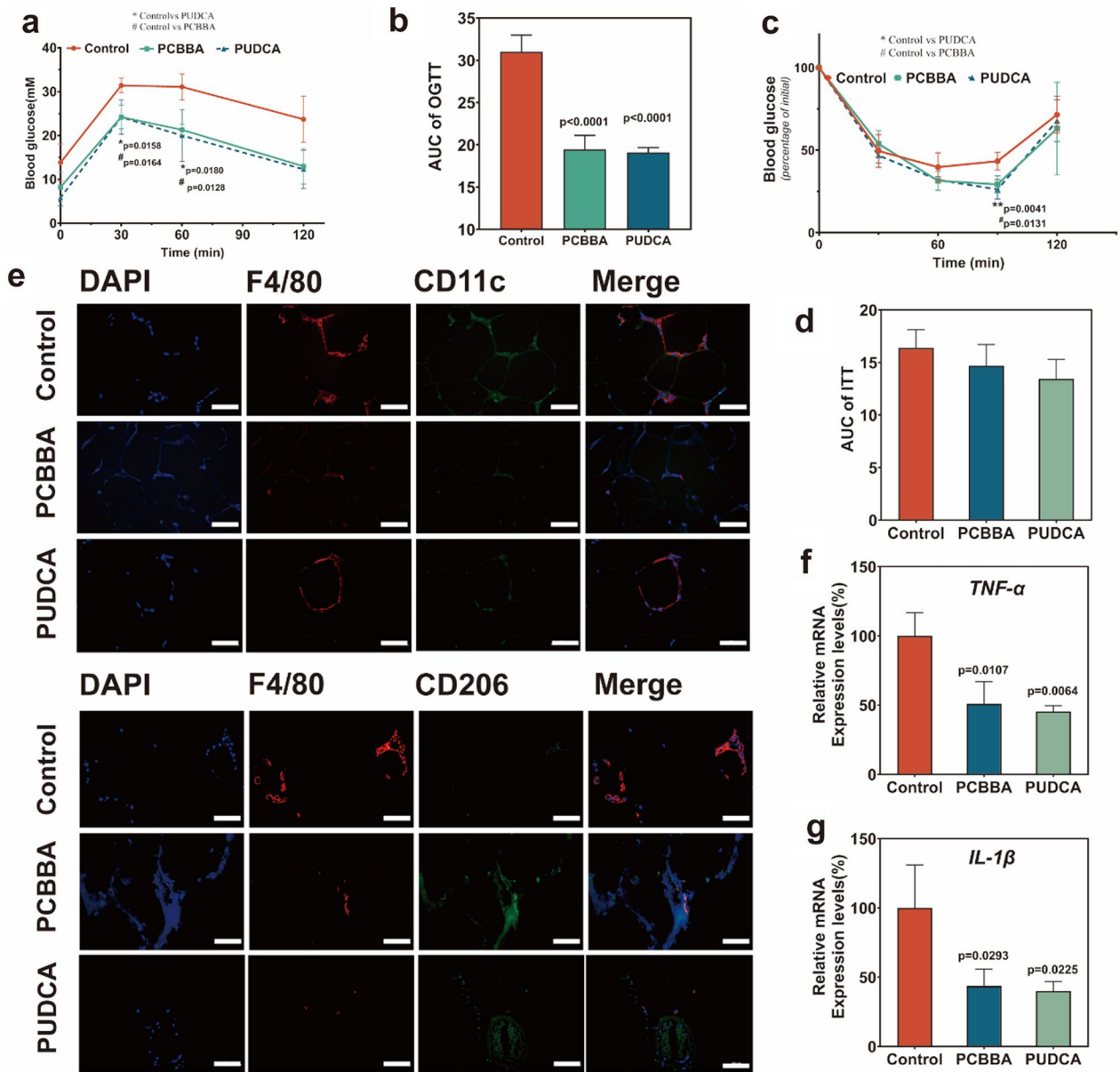


**Fig. 6** PCBBA alters WAT M1 and M2 macrophage polarization and improves insulin resistance in db/db mice. **a** Oral glucose tolerance test (OGTT) performed. **b** Area under the curve (AUC) quantification of blood glucose monitoring during OGTT. **c** Intraperitoneal insulin tolerance test (IPITT) performed. **d** AUC quantification of blood glucose monitoring during ITT. **e** Representative confocal images of WAT immunofluorescence staining with F4/80 (red), CD11c (green), CD206 (green), and DAPI (blue). F4/80<sup>+</sup>/CD11c<sup>+</sup> for M1-like type and F4/80<sup>+</sup>/CD206<sup>+</sup> for M2-like type. **f, g** The mRNA levels of proinflammatory factors in WAT were determined by quantitative real-time PCR analysis, the mRNA levels were normalized to that of β-actin mRNA by qPCR. (n=3 biologically independent samples, means ± SD. Scale bars, 50 μm. \*p < 0.05, \*\*p < 0.01, \*\*\*p < 0.001)

anti-inflammatory M2 phenotype releases a cascade of anti-inflammatory mediators that help maintain adipocyte sensitivity to insulin and suppress adipose tissue dysregulation and inflammation. Additionally, the reduction in adipocyte size, improvement in ectopic fat accumulation, and WAT browning collectively exert a beneficial effect on insulin resistance [81–83].

**PCBBA treatment reverses hepatic steatosis in db/db mice**  
 Obesity is frequently associated with hepatic steatosis, prompting us to investigate the effects of PCBBA treatment on liver pathology in db/db mice. After PCBBA administration, liver weight in treated mice was reduced by approximately one-third (Fig. 7a), and plasma levels of low-density lipoprotein cholesterol (LDL-C) significantly

decreased. Additionally, the levels of alanine aminotransferase (ALT) and aspartate aminotransferase (AST)—key markers of hepatic injury, often elevated due to liver inflammation and lipid accumulation—were notably reduced (Fig. 7b). To assess whether the decrease in ALT and AST was indicative of liver injury improvement, we performed histopathological imaging and qPCR analysis on liver tissues.

Histopathological analysis using H&E and Oil Red O staining showed that PCBBA ameliorated hepatic steatosis (Fig. 7d). Hepatic ballooning, characterized by microcysts and enlarged lipid droplets, was reduced in the PCBBA-treated group compared to the control group [84]. Additionally, the expression of fatty acid synthase (FASN), a gene associated with hepatic lipid accumulation, was significantly reduced, indicating normalization of hepatic metabolism (Fig. 7c).

Interestingly, no significant changes were observed in the expression of key metabolic regulators such as SREBP1c, PGC1 $\alpha$ , and PPAR $\alpha$ . This stability in expression may be attributed to the activation of the Farnesoid X Receptor (FXR), a receptor primarily expressed in the liver and intestines and activated by bile acids. FXR activation is known to produce beneficial metabolic effects, including reduced inflammation, increased insulin sensitivity, and lower ectopic triglyceride levels. Since FASN is a direct target gene of FXR, its downregulation likely occurs independently of SREBP1c involvement, indicating that FXR activation—mediated by PCBBA or PUDCA—was responsible for the observed improvements in liver lipid metabolism [85].

During liver injury, hepatic macrophages rapidly infiltrate the liver, and their phenotype and function are strongly influenced by the local tissue environment. These macrophages interact with various liver cell types and are critical in regulating liver injury, repair, and disease progression. Immunofluorescence staining revealed a significant increase in CD206<sup>+</sup> macrophages in the PCBBA-treated group, accompanied by a reduction in pro-inflammatory cytokines such as TNF- $\alpha$ , IL-6, and IL-1 $\beta$  (Fig. 7e and f).

In conclusion, these findings highlight the potential of PCBBA to modulate metabolic disease outcomes.

PCBBA not only inhibited lipid accumulation in hepatocytes but also reduced hepatic inflammation, leading to an overall improvement in symptoms of hepatic steatosis. Our results suggest that this therapeutic effect is largely attributed to the presence of bile acids in PCBBA. Notably, the effects of PCBBA and PUDCA were nearly identical in our experiments, indicating that both compounds may share similar activation pathways involving the bile acid receptors TGR5 and FXR.

### Biocompatibility and long-term safety

We conducted a comprehensive assessment of both the *in vitro* cell viability and the long-term *in vivo* safety profile of PCBBA. As shown in Fig. S12, all samples demonstrated negligible cytotoxicity within the concentration range of 0.01 to 1 mg/mL when tested on Caco-2 cells. To assess the potential for cell membrane disruption, PCBBA was incubated with erythrocytes for 4 h, revealing no significant hemolysis within the specified concentration range Fig. S13.

Furthermore, we explored the potential toxicity of PCBBA through a long-term dosing regimen, where healthy mice received oral PCBBA administration twice daily for 7 consecutive days. As illustrated in Fig. S14–17, small intestine tissue exhibited intact finger-like villi, as evidenced by Haematoxylin and eosin (H&E) staining. Additionally, there was no observable structural damage or significant inflammation in major organs or small intestine tissue. Markers related to liver, kidney, and other relevant functions did not exhibit significant differences compared to the control group. These findings collectively demonstrate the biosafety of PCBBA nanoparticles *in vivo*.

### Experimental methods

**Material:** All standard synthesis reagents were purchased from commercial suppliers and used without any further purification. Cell Counting Kit-8 (CCK-8) was purchased from Dojindo (Japan). 4',6-diamidino-2-phenylindole (DAPI), Trypsin–EDTA, Dulbecco's

(See figure on next page.)

**Fig. 7** PCBBA Enhances Lipid Metabolism and Reduces Inflammation in the Liver. **a** liver weight of db/db mice after oral administration every three days for 2 weeks. **b** Serum levels of alanine aminotransferase (ALT), aspartate aminotransferase (AST), and low-density lipoprotein cholesterol (LDL-C). **c** Relative mRNA expression levels of lipid metabolism markers (SREBP1c and FASN), and hepatic mitochondrial biogenesis markers (PGC1 $\alpha$  and PPAR $\alpha$ ) in the liver. The mRNA levels were normalized to that of  $\beta$ -actin mRNA by qPCR. **d** H&E staining and Oil Red O staining of the liver (Scale bars, 100  $\mu$ m). **e** The mRNA levels of proinflammatory factors in the liver were determined by quantitative real-time PCR analysis, and the mRNA levels were normalized to that of  $\beta$ -actin mRNA by qPCR. **f** Representative confocal images of liver immunofluorescence staining with F4/80 (red), CD11c (green), CD206 (green), and DAPI (blue). F4/80<sup>+</sup>/CD11c<sup>+</sup> for the M1-like type and F4/80<sup>+</sup>/CD206<sup>+</sup> for the M2-like type (Scale bars, 50  $\mu$ m). (n = 3 biologically independent samples, means  $\pm$  SD.)

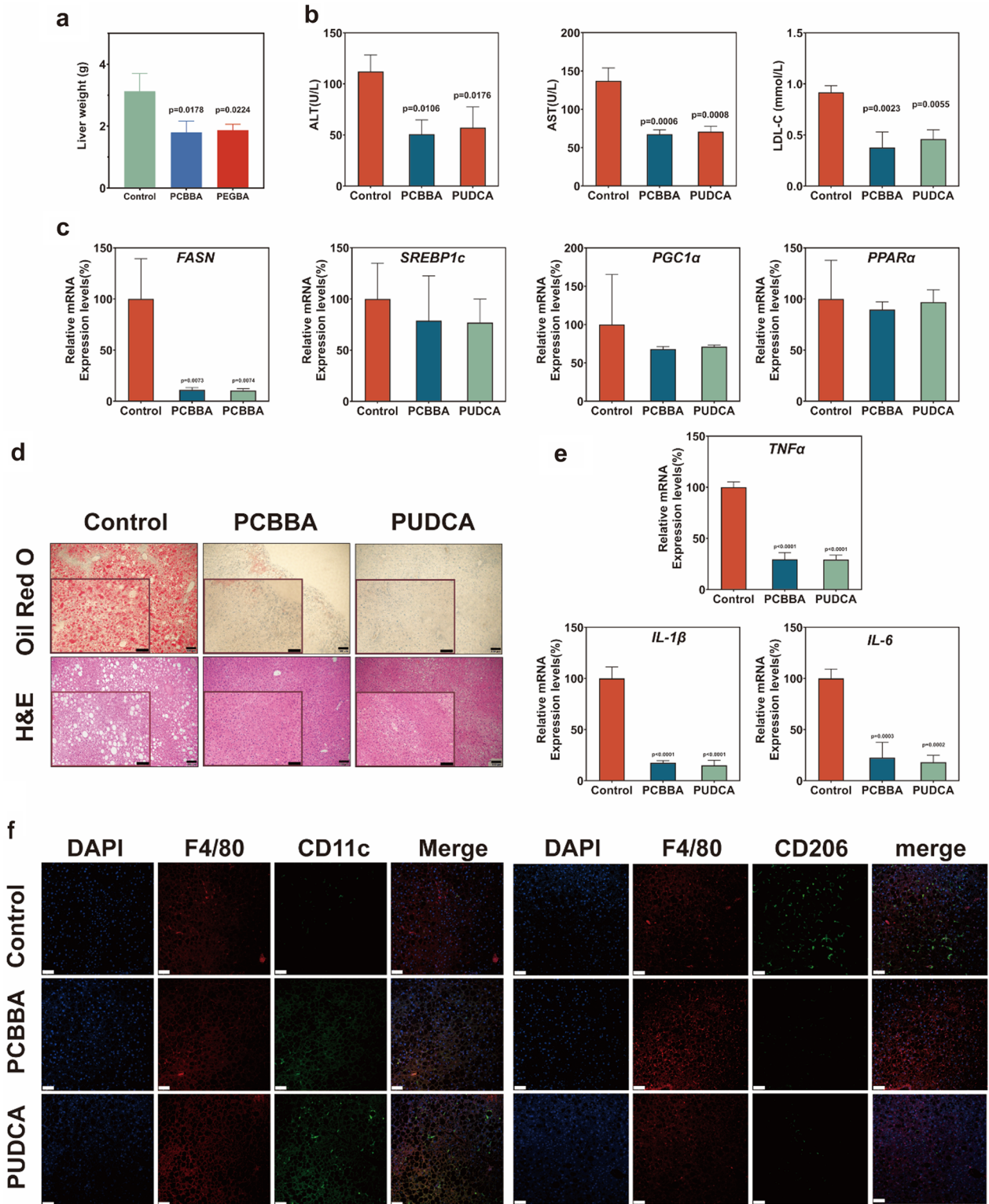


**Fig. 7** (See legend on previous page.)

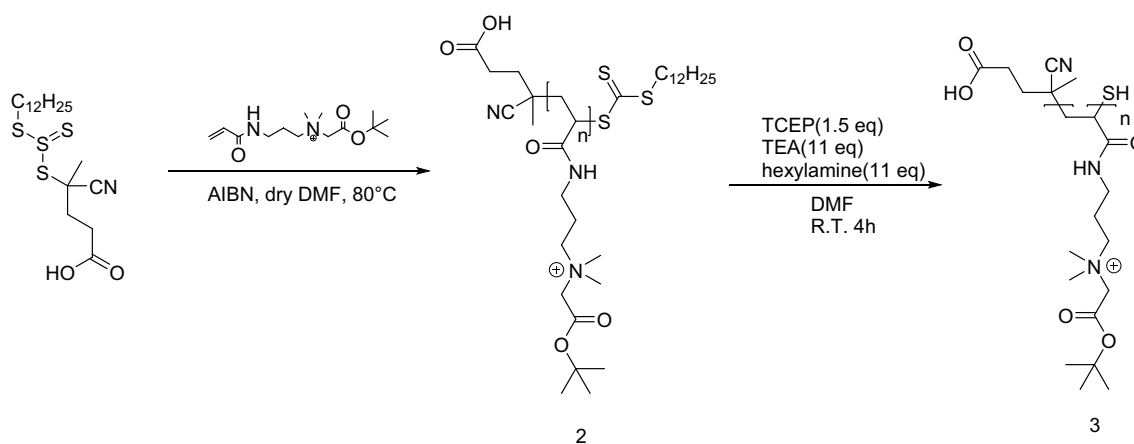
Phosphate Buffered Saline (PBS), Dulbecco's modified eagle's medium (DMEM) and fetal bovine serum (FBS Laboratories), were purchased from Thermo & Fisher Scientific. Streptozotocin (STZ), Insulin-FITC, mucin, and the BCA kit were purchased from Sigma-Aldrich (St. Louis, MO, USA). The Human Insulin ELISA Kit was purchased from Beyotime Biotechnology (Shanghai, China). Transwell® Permeable Supports (0.4 μm, Corning, USA), O.C.T gel (Tissue-Tek, Torrance, CA, USA). Monoclonal antibodies (FITC anti-mouse CD11c, FITC anti-mouse F4/80, APC anti-mouse CD206, anti-UCP1 antibody) were purchased from Abcam (China). Experimental consumables were mostly purchased from Corning (Corning, NY, USA), Titan (Shanghai, China), or BioFil (JET, Guangzhou, China).

**Characterization:** Transmission electron microscopy (TEM, Talos F200X G2) was used to characterize the morphology and size of the nanoparticle. Zetasizer (Malvern Zetasizer Nano) was used to measure the hydrodynamic size and zeta potential of nanoparticles. In vitro, a confocal imaging system (TCS SP8 STED 3X, Leica, Germany) was used to observe fluorescence in

All animals were housed in the Laboratory Animal Center of Shanghai Jiao Tong University under specific pathogen-free conditions. All animal experiments were performed according to the guidelines for the protection of animal life and protocols approved by the Laboratory Animal Ethics Committee at Shanghai Jiao Tong University.

### Synthesis of 3-acrylamido-N-(2-(tert-butoxy)-2-oxoethyl)-N,N-dimethylpropan-1-aminium (CB-tBu)

N,N-dimethylaminopropyl acrylamide (6 g, 38 mmol, 1 eq), and tert-butyl bromoacetate (8.5 mL, 57.6 mmol, 1.5 eq) were dissolved in acetonitrile (35 mL). The reaction mixture was stirred in a 60 °C oil bath for 12 h and then cooled to room temperature (RT). The product was then precipitated in diethyl ether, filtered via a fritted funnel, and dried under vacuum overnight to yield a white powder. Yield: 95%. <sup>1</sup>H NMR (400 MHz, Chloroform-d) δ 8.26 (t, J = 5.8 Hz, 1H), 6.49 (dd, J = 17.1, 10.2 Hz, 1H), 6.30 (dd, J = 17.1, 1.7 Hz, 1H), 5.63 (dd, J = 10.2, 1.7 Hz, 1H), 4.40 (s, 2H), 4.17–4.07 (m, 2H), 3.53–3.44 (m, 8H), 2.17 (m, 2H), 1.50 (s, 9H).



Caco-2 cells. In vivo, H&E and Oil Red O staining sections were observed under an automated fluorescence microscope (BX63, OLYMPUS, USA). The fluorescence images of mice were captured by IVIS spectrum (PerkinElmer, USA).

**Cell lines:** The human colon adenocarcinoma cell line (Caco-2) was purchased from the China Type Culture Collection. The Caco-2 cells were incubated in a nutritious DMEM medium (containing 10% FBS and 1% (v/v) penicillin–streptomycin) at 37 °C with 5% CO<sub>2</sub>.

**Mice:** BALB/c mice (male, 6 weeks old), BALB/c mice (female, 6 weeks old), and rat (Sprague Dawley rat, 6 weeks old, male), were purchased from SPF (Suzhou) Biotechnology Co., Ltd. BKS-DB mice (male, 5 weeks old) were purchased from Gempharmatech Co., Ltd.

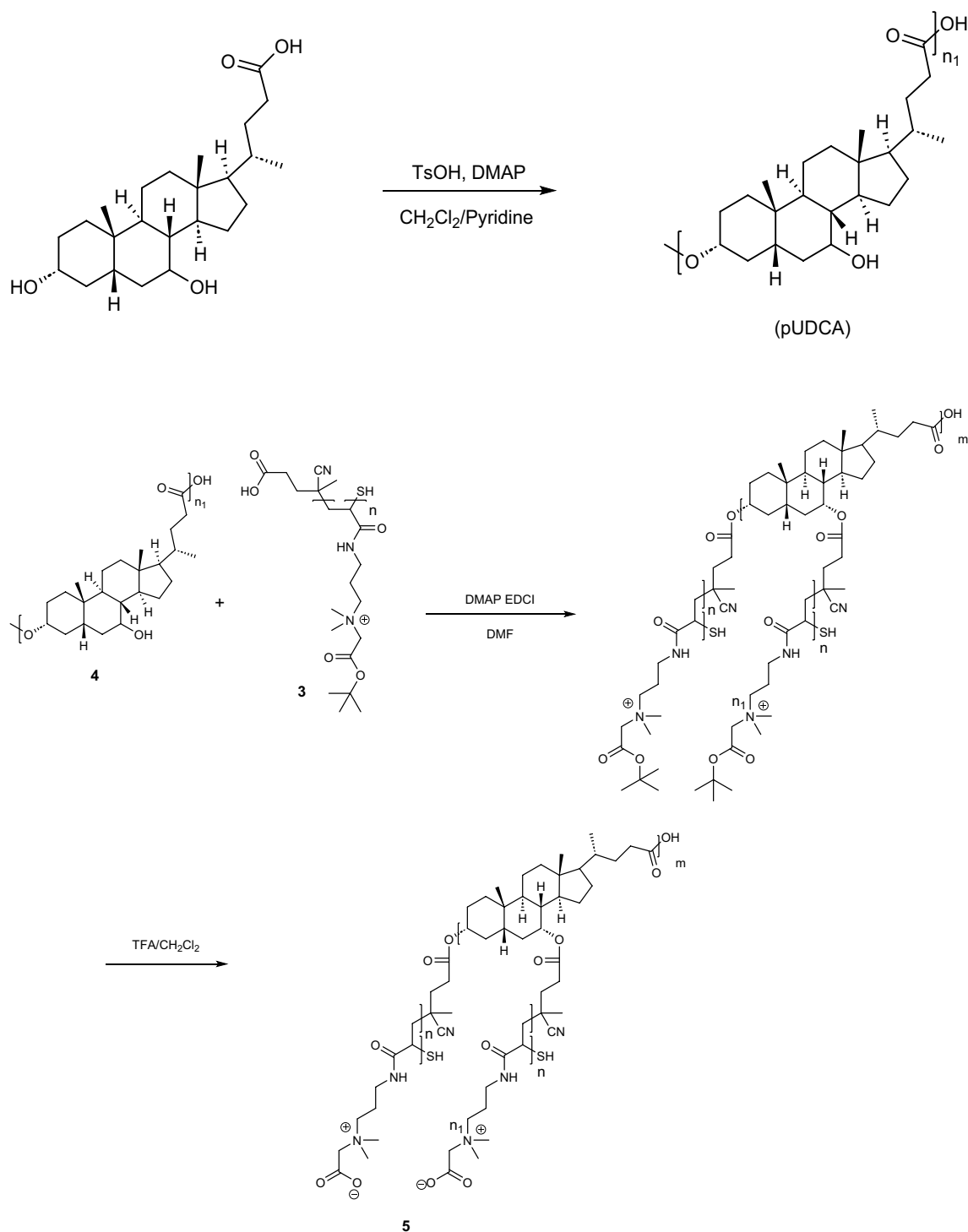
### Synthesis of PCB-tBu

4-Cyano-4-[(dodecylsulfanylthiocarbonyl) sulfanyl]pentanoic acid (CDP, 108 mg, 0.27 mmol, 1 eq.), CB-tBu (1.5 g, 5.4 mmol, 20 eq.), 4,4'-Azobis(4-cyanovaleric acid) (ACVA, 8.9 mg, 0.032 mmol, 0.1 eq.) were firstly dissolved in dimethylformamide (DMF, 35 mL) in a 100 mL flask. The flask was deoxygenated by cycling between nitrogen and vacuum three times, then transferred to an oil bath (70 °C) for 4 h. The resultant polymer (2) was precipitated in ice-cold ethyl acetate three times and dried under vacuum. Then triethylamine (TEA, 375 μL, 2.7 mmol, 10 eq), hexylamine (357 μL, 2.7 mmol, 10 eq), 2 (1.5 g, 0.27 mmol, 1 eq), and tris(2-carboxyethyl)phosphine hydrochloride (TCEP, 115 mg, 0.4 mmol, 1.5 eq)

were dissolved in DMF(10 mL). After being stirred at RT for 4 h, the color of the reaction solution turned colorless. Then, the mixture was precipitated in ice-cold ethyl acetate and dried under vacuum to afford compound 3.  $^1\text{H}$  NMR (400 MHz, Chloroform- $d$ )  $\delta$  0.83–0.93, 1.2–1.3, 1.4–1.7, 1.9–2.4, 3.1–3.7, 3.7–4.2, 4.3–4.8

### Synthesis of PCBBA

Bile-acid polymers(pBA) were synthesized according to literature reports. Briefly, bile acids (5.4 mmol), paratoluenesulfonic acid (0.652 mmol), and dimethylaminopyridine (0.652 mmol) were dissolved in 60 mL 5:1



anhydrous methylene chloride to anhydrous pyridine solvent mixture and stirred at 40 °C. To the reaction mixture, diisopropyl carbodiimide (6.92 mmol) was added and the reaction mixture was stirred at 40 °C for 4 h in the nitrogen atmosphere. The polyester product, pBA, was precipitated into 400 mL cold ethyl acetate collected by centrifugation (Centrifuge 5810 R, Eppendorf) and dried to retain a white powder. Polymerization was confirmed by <sup>1</sup>H NMR.

PCB (1.0 eq), EDCI (1.2 eq), and DMAP (0.1 eq) were dissolved in anhydrous dichloromethane and added to pUDCA (1.0 eq) under nitrogen protection. The reaction mixture was stirred at room temperature overnight. The mixture was precipitated into cold ethyl acetate collected by centrifugation (Centrifuge 5810 R, Eppendorf) and dried to obtain a white powder. To a mixture of intermediate PCBBA-tBu in DCM (4 mL), TFA (4 mL) was added and stirred at 25 °C for 4 h. When the reaction was complete, the crude mixture was evaporated under reduced pressure, and the residue was purified by freeze-drying to obtain target compounds (5).

#### Preparation and characterization of blank nanoparticles

15 mg of PCBBA was dissolved in 1 mL of PBS under stirring at room temperature for 2 h. Then blank nanoparticles were further purified through ultrafiltration (Millipore, molecular weight cutoff (MWCO) = 10 kDa) to remove rough materials and a 0.22 μm filter (BIOFIL) to remove unexpected large particles. The size, PDI, and zeta potential of the nanoparticles were measured with Malvern Zetasizer Nano (Nano-ZS90). PEGBA nanoparticles were prepared using the same approach.

#### Preparation and characterization of drug-loaded nanoparticles and oral PCBBA capsules

10 mg of PCBBA was added to 1 mL of an insulin solution (1 mg/mL, dissolved in PBS). Then 200 μL of ZnCl<sub>2</sub> solution (2 mg/mL) was added dropwise to the insulin-containing mixture. The mixture was stirred at room temperature for 2 h. Subsequently, drug-loaded nanoparticles were purified using ultrafiltration (Millipore, MWCO 10 kDa) to remove coarse materials and a 0.22 μm filter to eliminate large particles. The size, PDI, and zeta potential of the nanoparticles were measured using a Malvern Zetasizer Nano. The nanoparticles were then further purified by ultrafiltration (Millipore, MWCO 50 kDa) to remove free insulin, and the insulin content was determined using the BCA Protein Assay Kit (Sigma-Aldrich). PCBBA-FITC-ins nanoparticles were also prepared using the same method. Encapsulation

efficiency and drug loading efficiency were calculated by the following equations:

$$\text{Encapsulation efficiency(\%)} = \left( \frac{\text{amount of insulin in the nanoparticles}}{\text{amount of insulin}} \right) \times 100\%$$

$$\text{Loading efficiency(\%)} = \left( \frac{\text{amount of insulin in the nanoparticles}}{\text{amount of drug} - \text{loaded nanoparticles}} \right) \times 100\%$$

The PCBBA-Ins nanoparticles were lyophilized into a solid powder to prepare oral capsules and encapsulated in enteric gel capsules. The amount of PCBBA-Ins nanoparticles per capsule was adjusted according to the target animal weight.

#### Transmission electron microscopy (TEM)

The use of transmission electron microscopy to observe the morphology of nanoparticles with the specific preparation method: the copper mesh coated with carbon film immersed in the suspension of NPs. Stain the nanoparticles with a 2% phosphotungstate solution, then dry the copper mesh at room temperature. TEM (Tecnai G2, Thermofisher) determines the size and morphology of NPs.

#### In vitro stability of nanoparticles

The blank nanoparticles were stored at room temperature (25 °C) and 4 °C for long-term stability studies. At timed intervals, nanoparticles' particle size, PDI, and zeta potential were measured with Malvern Zetasizer Nano (Nano-ZS90).

#### In vitro drug release study

To test the release behaviors of Insulin-loaded nanoparticles, samples were placed in dialysis bags (MWCO 10 kDa) and dispersed in simulated gastric fluid (SGF, Shanghai YuanYe Bio-Technology, China), simulated intestine fluid (SIF, Shanghai YuanYe Bio-Technology, China), and PBS at 37 °C for 24 h. At timed intervals, 100 μL of buffer was taken, and an equal volume of fresh buffer was added to ensure a constant volume. The content of insulin was detected by the BCA kit (Sigma-Aldrich).

#### In vitro gastrointestinal stability studies

PCBBA-ins and free insulin were added to simulated gastric fluid (SGF) or small intestinal fluid (SIF) containing 10 mg/mL of trypsin, with a final insulin concentration of 300 μg/mL. The mixtures were incubated at 37 °C, and 100 μL samples were collected at predetermined intervals, with the same volume of medium replenished after

each collection. Insulin activity in the samples was subsequently measured using ELISA.

#### Mucus penetration studies

40  $\mu\text{L}$  of a 6% (m/v) mucin (Sigma-Aldrich) solution is added to the upper chamber of a transwell's polycarbonate cell culture (0.4  $\mu\text{m}$ , Corning, USA) insert and shaken smoothly until the solution is flat. Then 40  $\mu\text{L}$  of FITC-INS/PCBBA nanoparticles at the same concentration is carefully added on top of the mucin solution of the insert. At predetermined time intervals, the solution from the basolateral chamber is collected to detect fluorescence intensity. Then Permeability coefficient ( $P_{\text{app}}$ ) was calculated by the following equations:

$$\text{Permeability coefficient}(\%) = \frac{Q}{A \times C \times t}$$

#### Cell viability assay

Blank nanoparticles with different concentrations were added into 96-well plates filled with Caco-2 cells (5000 cells per well) and then cultured for 4 h. Subsequently, the CCK-8 solution was added to react for 2 h. The OD values in each well were measured at 450 nm and 630 nm using a microplate spectrophotometer (SpectraMax, Molecular Devices). Cell viability was calculated from the following equation,

$$\text{Cell viability}(\%) = \left( \frac{OD_{\text{sample}} - OD_{\text{blank}}}{OD_{\text{control}} - OD_{\text{blank}}} \right) \times 100\%$$

#### Hemolysis test

Fresh blood from mice was centrifuged at 1500 rpm for 5 min in a centrifuge tube containing anticoagulant, and the supernatant was slowly aspirated off. The PBS wash step was repeated two to three times. The erythrocyte precipitate was gently dispersed with PBS and mixed with different concentrations of nanoparticles in PBS. The erythrocytes were mixed with deionized water in the positive group and PBS in the negative group, respectively. All groups were incubated at 37  $^{\circ}\text{C}$  for 4 h and centrifuged after completion of incubation. The UV absorption value of the supernatant at 540 nm was measured, and the hemolysis rate of the samples was calculated according to the formula.

$$\text{Hemolysis}(\%) = \left( \frac{A_{\text{sample}} - A_{\text{negative}}}{A_{\text{positive}} - A_{\text{negative}}} \right) \times 100\%$$

#### Endocytosis and exocytosis kinetic of PCBBA nanoparticles

**Endocytosis:** Cells were plated into a 12-well plate ( $1 \times 10^5$  cells per well) and then pre-treated with different

Endocytosis inhibitors (wortmannin (5  $\mu\text{M}$ ), chlorpromazine (30  $\mu\text{M}$ ), Genistein (35  $\mu\text{M}$ ), Titan, Shanghai, China) for 2 h. After incubation, the PCBBA-FITC-ins nanoparticles (insulin-equiv. concentration of 50  $\mu\text{g}/\text{mL}$ ) were added to the plates and co-cultured for 1 h. After incubation, the cells were washed several times with PBS to remove the free PCBBA-FITC-ins nanoparticles. The cell suspension was collected and analyzed by flow cytometry. Every 10000 cells were counted to determine FITC-positive cells.

**Exocytosis kinetic:** Cells were seeded on a 12-well plate ( $1 \times 10^5$  cells per well) and then incubated with the PCBBA-FITC-ins nanoparticles (insulin-equiv. concentration of 50  $\mu\text{g}/\text{mL}$ ) for 3 h. After incubation, the cells were washed several times with PBS to remove the free PCBBA-FITC-ins nanoparticles and re-cultured with different exocytosis inhibitors (monensin (50  $\mu\text{M}$ ), nocodazole (30  $\mu\text{M}$ ), Titan, Shanghai, China) for 6 h. In addition, the plates were placed in a 4  $^{\circ}\text{C}$  refrigerator to complete the temperature effect experiment. After incubation, the cell suspension was collected and analyzed by flow cytometry. Every 10,000 cells were counted to determine FITC-positive cells.

These experiments were repeated three times independently; data were presented as mean  $\pm$  SD. FlowJo software was used for analysis.

#### Establishment of diabetic mice model

All animals were housed in the Laboratory Animal Center of Shanghai Jiao Tong University under specific pathogen-free conditions. All animal experiments were performed according to the guidelines for the protection of animal life and protocols approved by the Laboratory Animal Ethics Committee at Shanghai Jiao Tong University.

After the mice (male, 6 weeks old, SPF (Suzhou) Biotechnology Co., Ltd) were fasted overnight, STZ (60 mg/kg, Sigma-Aldrich) was injected intraperitoneally into the healthy BALB/c mice for 10 consecutive days. During the period, the mice's body weight and blood glucose changes were monitored daily to confirm their diabetic status. Diabetic mice with blood glucose above 11 mmol/liter were selected for further in vivo testing (Fig. S13).

#### Hypoglycemic response in vivo

Following 4 h of fasting, diabetic mice were orally gavaged with PCBBA/insulin (30 IU/kg) or PEGBA/insulin (30 IU/kg). As control groups, one group of diabetic mice was administered free insulin (30 IU/kg) and PBS by oral gavage, and the other group was administered free insulin (5 IU/kg) by subcutaneous injection. Blood samples were collected from the tails at predetermined time

intervals and analyzed using a blood glucose meter (sinocare, China).

Following 4 h of fasting, healthy mice (female, 30–45 g to ensure that sufficient blood samples can be taken, SPF (Suzhou) Biotechnology Co., Ltd) were randomly divided into three groups including free insulin (30 IU/kg, p.o.), PCBBA/insulin (30 IU/kg, p.o.) and free insulin (3 IU/kg, S.C.). Blood samples were collected from the tails at predetermined intervals and analyzed using a blood glucose meter. The insulin contents in blood samples were measured using the Human Insulin ELISA Kit (Beyotime). The area above the curve (AAC) of the blood glucose level and the area under the curve (AUC) of plasma insulin concentration were computed.

Following 4 h of fasting, healthy rats (Sprague Dawley rat, 6 weeks old, male, 280–300 g) were randomly divided into three groups including insulin capsules (10 IU/kg, p.o.), PCBBA/insulin capsules (10 IU/kg, p.o.), and free insulin (5 IU/kg, S.C.). Blood samples were collected at predetermined time intervals. The insulin contents in blood samples were measured using the Human Insulin ELISA Kit (Beyotime).

The area under the curve (AUC) of plasma insulin concentration was computed. Oral bioavailability (F%) was quantitated relative to a subcutaneous injection using the following equations:

$$F(\%) = (AUC_{\text{oral}} \times \text{Dose}_{\text{s.c.}}) / (AUC_{\text{s.c.}} \times \text{Dose}_{\text{oral}}) \times 100\%$$

#### Absorption sites and kinetics of orally delivered insulin

Healthy mice were fasted overnight and then administered with free FITC-insulin PCBBA/FITC-insulin or PEGBA/FITC-insulin by oral gavage (100  $\mu$ L; insulin-equiv. concentration, 1 mg/mL). At timed intervals, the mice were anesthetized and then visualized by the IVIS Spectrum system. At the fourth hour after administration, three mice were sacrificed by cervical dislocation and the whole gastrointestinal tract and vital organs (heart, liver, spleen, lungs, kidneys, Pancreas) were excised and imaged by the IVIS Spectrum system (PerkinElmer, USA). The fluorescence intensities were quantified with Living Image<sup>®</sup>.

#### Experiments with db/db diabetic animal models

To evaluate the preventive and therapeutic effects of PCBBA nanoparticles on obesity and diabetes, diabetic mice (BKS-DB mice, male, 5 weeks old, Gempharmatech Co., Ltd) were divided into three groups: (1) PBS, (2) oral PCBBA group (50 mg/kg), and (3) PUDCA (10 mg/kg). The different formulations were given every three days for two weeks, and the mice were tested for body weight and blood glucose two weeks later. Then, the mice were

sacrificed and the hearts, livers, spleens, lungs, kidneys, and white adipose tissue (WAT, subcutaneous WAT and mesenteric WAT tissue) samples were collected. The livers and WAT of the mice were weighed, and then the hearts, livers, spleens, lungs, kidneys and WAT of the mice were sectioned for H&E staining. In addition, the livers were stained for Oil Red O staining to stain the fat droplets red. To observe the switch in adipose tissue macrophage polarization, immunofluorescence staining was used to localize distinct ATM subsets within adipose tissue.

#### Oral glucose tolerance test (OGTT) and insulin tolerance test (ITT)

The mice were fasted overnight before the experiment, followed by a glucose tolerance test. First, blood was taken from the tail vein, and blood glucose levels were measured with a glucometer. Then, each mouse was given 1 g/kg glucose orally. The blood glucose levels of the mice were measured at a specified time.

The mice were fasted for 4 h before the experiment and blood glucose levels were measured before the start of the experiment, then 2 IU/kg insulin was injected subcutaneously into the mice. Blood glucose levels were measured at the specified time.

#### RNA extraction and quantitative real-time PCR

Total RNA was extracted from tissues using Trizol reagent, and its concentration was measured with a Nanodrop One spectrophotometer (Thermo). cDNA synthesis from RNA was performed using the HiScript III RT SuperMix cDNA Synthesis Kit (Vazyme, China). Real-time quantitative PCR mixtures were prepared with ChamQ Universal SYBR qPCR Master Mix according to the manufacturer's instructions, and all reactions were conducted in triplicate on a CFX Opus96 system (BIO-RAD). Primer sequences for the target genes are listed in Table S1, Supporting Information. The relative abundance of each gene was normalized to the mRNA level of actin.

#### Toxicity evaluation

Healthy BALB/c mice were randomly divided into three groups (n = 3) and were administered with PBS, PCBBA nanoparticles and PEGBA nanoparticles through gavage (0.53 mg of PCBBA or PEGBA per mouse) twice daily for 7 consecutive days. After the last treatment, the Serum of each mouse was collected for biochemistry analysis. Biochemistry index, including total protein (TP), albumin (ALB), globulin (GLB), direct bilirubin (DBILI), indirect

bilirubin (IBIL), alanine aminotransferase (ALT), aspartate aminotransferase (AST), alkaline phosphatase (ALP), creatinine (CRE), uric acid (UA), blood urea nitrogen (BUN) and hypersensitive C-reactive protein (CRP), were detected to indicate liver function and kidney function, respectively. Meanwhile, hearts, livers, spleens, lungs, kidneys and intestines were excised and sectioned for H&E staining.

### Statistical analyses

The results were analyzed using Prism 8 (Graph-Pad Software Inc., CA, USA), and the data are presented as the mean  $\pm$  standard deviation (SD). Statistical significance was determined by unpaired two-tailed Student's t-tests where only two groups existed or by ANOVA tests with Dunnett's or Tukey's post-test.  $p < 0.05$  was considered to be statistically significant, (\* $p < 0.05$ , \*\* $p < 0.01$ , \*\*\* $p < 0.001$ , \*\*\*\* $p < 0.0001$ ); n.s., no significance. Sample size (n) and preprocessing normalization of data were given in the corresponding figure legend.

### Conclusion

In this study, we designed and synthesized an amphiphilic polymer composed of a hydrophilic polyzwitterion and a hydrophobic bile acid polymer. The resulting PCBBA nanoparticles exhibited an exceptional ability to penetrate mucosal barriers and intestinal epithelial cells, enabling efficient insulin delivery into the bloodstream and significantly improving oral insulin bioavailability. This hypoglycemic effect was observed in healthy mice, STZ-induced type 1 diabetic mice, db/db mice, and rats, with oral bioavailability exceeding 30% when delivered via enteric-coated capsules. Furthermore, PCBBA treatment reduced weight gain, with treated mice averaging 81% of the control group's weight. PCBBA also regulated lipid metabolism and alleviated inflammation in both adipose and liver tissues, contributing to broader metabolic benefits. These effects appear to be closely linked to the presence of bile acids in PCBBA, highlighting the critical role of bile acids in managing metabolic conditions, including weight loss.

PCBBA nanoparticles are easy to prepare using biocompatible bile acids and betaines, and they exhibited no significant toxicity in animal models. As an innovative oral delivery system, PCBBA offers an effective means of controlling blood glucose levels via oral insulin administration and holds promise for the prevention and treatment of obesity, inflammation, and related metabolic complications in diabetic patients. However, further studies are needed to validate this nanosystem's efficacy in larger animal models. Ongoing research aims to explore the underlying mechanisms of PCBBA-induced weight loss in greater detail. In conclusion, this oral

formulation demonstrated high bioavailability, excellent biosafety, and efficacy in managing diabetes and associated metabolic disorders, presenting a promising therapeutic strategy for diabetic patients.

### Supplementary Information

The online version contains supplementary material available at <https://doi.org/10.1186/s12951-025-03190-8>.

Supplementary Material 1.

### Acknowledgements

This study was supported by National Natural Science Foundation of China (No. 82173770) and the Fundamental Research Funds for the Central Universities (YG2023QNA37). The authors appreciate the help from the faculties of Instrumental Analysis Centre (IAC) of Shanghai Jiao Tong University.

### Author contributions

W-E.Y: conceived the initial idea and the conceptualization. W-E.Y. and W.Z: conceived the study design and participated in the data analysis and revised the manuscript. W.Z., Y.W., X.Z., Y.Z., W.Y. and H.T: participated in the study design, searched databases, extracted and assessed studies, and helped draft the manuscript. W.Z: wrote the manuscript, and W-E.Y: revised the manuscript. All authors have read and approved the final manuscript.

### Data availability

The datasets used and/or analyzed during the current study are available from the corresponding author on reasonable request or Data is provided within the manuscript or supplementary information files.

### Declarations

#### Ethics approval and consent to participate

All experiments involving animals were conducted according to the ethical policies and procedures approved by the ethics committee of Institutional Animal Care and Use Committee (IACUC) of Shanghai Jiao Tong University (Approval no. A2023207-001).

#### Competing interests

The authors declare no competing interests.

#### Author details

<sup>1</sup>Shanghai Frontiers Science Center of Drug Target Identification and Delivery, School of Pharmaceutical Sciences, Shanghai Jiao Tong University, Shanghai 200240, China. <sup>2</sup>Engineering Research Center of Cell & Therapeutic Antibody, Ministry of Education, School of Pharmacy, Shanghai Jiao Tong University, Shanghai 200240, China. <sup>3</sup>National Key Laboratory of Innovative Immunotherapy, Shanghai Jiao Tong University, Shanghai 200240, China. <sup>4</sup>Inner Mongolia Research Institute of Shanghai Jiao Tong University, Hohhot 010070, China. <sup>5</sup>Department of Bone and Joint Surgery, Department of Orthopedics, Renji Hospital, School of Medicine, Shanghai Jiao Tong University, 145 Shandong Middle Road, Shanghai 200001, China.

Received: 5 November 2024 Accepted: 1 February 2025

Published online: 22 February 2025

### References

1. Sun H, Saedi P, Karuranga S, Pinkepank M, Ogurtsova K, Duncan BB, et al. IDF diabetes atlas: global, regional and country-level diabetes prevalence estimates for 2021 and projections for 2045. *Diabete Res Clin Pract*. 2022;183: 109119.
2. Li Y, Teng D, Shi X, Qin G, Qin Y, Quan H, et al. Prevalence of diabetes recorded in mainland China using 2018 diagnostic criteria from the

- American diabetes association: national cross sectional study. *BMJ*. 2020;369: m997.
- Baryakova TH, Pogostin BH, Langer R, McHugh KJ. Overcoming barriers to patient adherence: the case for developing innovative drug delivery systems. *Nat Rev Drug Discov*. 2023;22:387–409.
  - ElSayed NA, Aleppo G, Aroda VR, Bannuru RR, Brown FM, Bruemmer D, et al. 9. Pharmacologic approaches to glycemic treatment: standards of care in diabetes—2023. *Diabetes Care*. 2022;46:S140–157.
  - US Food and Drug Administration. Novel drug approvals for 2023. FDA. 2023. <https://www.fda.gov/drugs/new-drugs-fda-cders-new-molecular-entities-and-new-therapeutic-biological-products/novel-drug-approvals-2023>.
  - Kulchar RJ, Singh R, Ding S, Alexander E, Leong KW, Daniell H. Delivery of biologics: topical administration. *Biomaterials*. 2023;302: 122312.
  - Brown TD, Whitehead KA, Mitragotri S. Materials for oral delivery of proteins and peptides. *Nat Rev Mater*. 2020;5:127–48.
  - Drucker DJ. Advances in oral peptide therapeutics. *Nat Rev Drug Discov*. 2020;19:277–89.
  - Argoud GM, Schade DS, Eaton RP. Insulin suppresses its own secretion in vivo. *Diabetes*. 1987;36:959–62.
  - Davies MJ, Aroda VR, Collins BS, Gabbay RA, Green J, Maruthur NM, et al. Management of hyperglycemia in type 2 diabetes, 2022. a consensus report by the american diabetes association (ADA) and the European association for the study of diabetes (EASD). *Diabetes Care*. 2022;45:2753–86.
  - Lingvay I, Sumithran P, Cohen RV, Le Roux CW. Obesity management as a primary treatment goal for type 2 diabetes: time to reframe the conversation. *Lancet*. 2022;399:394–405.
  - Haddadzadegan S, Dorkoosh F, Bernkop-Schnürch A. Oral delivery of therapeutic peptides and proteins: technology landscape of lipid-based nanocarriers. *Adv Drug Deliv Rev*. 2022;182: 114097.
  - Ensign LM, Cone R, Hanes J. Oral drug delivery with polymeric nanoparticles: the gastrointestinal mucus barriers. *Adv Drug Deliv Rev*. 2012;64:557–70.
  - Ouyang J, Zhang Z, Deng B, Liu J, Wang L, Liu H, et al. Oral drug delivery platforms for biomedical applications. *Mater Today*. 2023;62:296–326.
  - Tong T, Wang L, You X, Wu J. Nano and microscale delivery platforms for enhanced oral peptide/protein bioavailability. *Biomater Sci*. 2020;8:5804–23.
  - Zhang Y, Xiong GM, Ali Y, Boehm BO, Huang YY, Venkatraman S. Layer-by-layer coated nanoliposomes for oral delivery of insulin. *Nanoscale*. 2021;13:776–89.
  - Wright L, Barnes TJ, Prestidge CA. Oral delivery of protein-based therapeutics: gastroprotective strategies, physiological barriers and in vitro permeability prediction. *Int J Pharm*. 2020;585: 119488.
  - Deng B, Liu S, Wang Y, Ali B, Kong N, Xie T, et al. Oral nanomedicine: challenges and opportunities. *Adv Mater*. 2024;36:2306081.
  - Chiang JYL. Bile acid metabolism and signaling. *Compr Physiol*. 2013;3:1191–212.
  - McGloone ER, Bloom SR. Bile acids and the metabolic syndrome. *Ann Clin Biochem*. 2019;56:326–37.
  - Molinaro A, Wahlström A, Marschall HU. Role of bile acids in metabolic control. *Trends Endocrinol Metab*. 2018;29:31–41.
  - Zheng X, Chen T, Jiang R, Zhao A, Wu Q, Kuang J, et al. Hycocholic acid species improve glucose homeostasis through a distinct TGR5 and FXR signaling mechanism. *Cell Metab*. 2021;33:791–803.e7.
  - Chávez-Talavera O, Haas J, Grzych G, Tailleux A, Staels B. Bile acid alterations in nonalcoholic fatty liver disease, obesity, insulin resistance and type 2 diabetes: what do the human studies tell? *Curr Opin Lipidol*. 2019;30:244.
  - Perino A, Schoonjans K. Metabolic messengers: bile acids. *Nat Metab*. 2022;4:416–23.
  - Watanabe M, Houten SM, Matakic C, Christoffolete MA, Kim BW, Sato H, et al. Bile acids induce energy expenditure by promoting intracellular thyroid hormone activation. *Nature*. 2006;439:484–9.
  - Ferrell JM, Chiang JYL. Understanding bile acid signaling in diabetes: from pathophysiology to therapeutic targets. *Diabetes Metab J*. 2019;43:257–72.
  - Mueller M, Thorell A, Claudel T, Jha P, Koefeler H, Lackner C, et al. Ursodeoxycholic acid exerts farnesoid X receptor-antagonistic effects on bile acid and lipid metabolism in morbid obesity. *J Hepatol*. 2015;62:1398–404.
  - Deng F, Bae YH. Bile acid transporter-mediated oral drug delivery. *J Control Release*. 2020;327:100–16.
  - Faustino C, Serafim C, Rijo P, Reis CP. Bile acids and bile acid derivatives: use in drug delivery systems and as therapeutic agents. *Expert Opin Drug Deliv*. 2016;13:1133–48.
  - Le Dévédec F, Strandman S, Hildgen P, Leclair G, Zhu XX. PEGylated bile acids for use in drug delivery systems: enhanced solubility and bioavailability of itraconazole. *Mol Pharm*. 2013;10:3057–66.
  - Wu S, Sun C. A delivery system for oral administration of proteins/peptides through bile acid transport channels. *J Pharm Sci*. 2019;108:2143–52.
  - Deng F, Bae YH. Effect of modification of polystyrene nanoparticles with different bile acids on their oral transport. *Nanomedicine*. 2023;48: 102629.
  - Deng F, Kim KS, Moon J, Bae YH. Bile acid conjugation on solid nanoparticles enhances asbt-mediated endocytosis and chylomicron pathway but weakens the transcytosis by inducing transport flow in a cellular negative feedback loop. *Adv Sci*. 2022;9:2201414.
  - García KP, Zarschler K, Barbaro L, Barreto JA, O'Malley W, Spiccia L, et al. Zwitterionic-coated “stealth” nanoparticles for biomedical applications: recent advances in countering biomolecular corona formation and uptake by the mononuclear phagocyte system. *Small*. 2014;10:2516–29.
  - Zhou LY, Zhu YH, Wang XY, Shen C, Wei XW, Xu T, et al. Novel zwitterionic vectors: Multi-functional delivery systems for therapeutic genes and drugs. *Comput Struct Biotechnol J*. 2020;18:1980–99.
  - Chen S, Zhong Y, Fan W, Xiang J, Wang G, Zhou Q, et al. Enhanced tumour penetration and prolonged circulation in blood of polyzwitterion–drug conjugates with cell-membrane affinity. *Nat Biomed Eng*. 2021;5:1019–37.
  - Liu S, Wang X, Yu X, Cheng Q, Johnson LT, Chatterjee S, et al. Zwitterionic phospholipidation of cationic polymers facilitates systemic mRNA delivery to spleen and lymph nodes. *J Am Chem Soc*. 2021;143:21321–30.
  - Biosca A, Cabanach P, Abdulkarim M, Gumbleton M, Gómez-Canela C, Ramírez M, et al. Zwitterionic self-assembled nanoparticles as carriers for Plasmodium targeting in malaria oral treatment. *J Control Release*. 2021;331:364–75.
  - Erfani A, Seaberg J, Aichele CP, Ramsey JD. Interactions between biomolecules and zwitterionic moieties: a review. *Biomacromol*. 2020;21:2557–73.
  - Fang H, Chen L, Deng Z, Gao Y, Yang Y, Chen Q, et al. In situ polymerization of zwitterions on therapeutic proteins to enable their effective oral delivery. *ACS Nano*. 2023;17:1128–43.
  - Ji K, Wei X, Kahkoska AR, Zhang J, Zhang Y, Xu J, et al. An orally administered glucose-responsive polymeric complex for high-efficiency and safe delivery of insulin in mice and pigs. *Nat Nanotechnol*. 2024. <https://doi.org/10.1038/s41565-024-01764-5>.
  - Han X, Lu Y, Xie J, Zhang E, Zhu H, Du H, et al. Zwitterionic micelles efficiently deliver oral insulin without opening tight junctions. *Nat Nanotechnol*. 2020;15:605–14.
  - Shan W, Zhu X, Tao W, Cui Y, Liu M, Wu L, et al. Enhanced oral delivery of protein drugs using zwitterion-functionalized nanoparticles to overcome both the diffusion and absorption barriers. *ACS Appl Mater Interfac*. 2016;8:25444–53.
  - Zeng X, Tao W, Mei L, Huang L, Tan C, Feng S-S. Cholic acid-functionalized nanoparticles of star-shaped PLGA-vitamin E TPGS copolymer for docetaxel delivery to cervical cancer. *Biomaterials*. 2013;34:6058–67.
  - Fan W, Xia D, Zhu Q, Li X, He S, Zhu C, et al. Functional nanoparticles exploit the bile acid pathway to overcome multiple barriers of the intestinal epithelium for oral insulin delivery. *Biomaterials*. 2018;151:13–23.
  - Lee JS, Han P, Chaudhury R, Khan S, Bickerton S, McHugh MD, et al. Metabolic and immunomodulatory control of type 1 diabetes via orally delivered bile-acid-polymer nanocarriers of insulin or rapamycin. *Nat Biomed Eng*. 2021;5:983–97.
  - Qian H, Wang K, Lv M, Zhao C, Wang H, Wen S, et al. Recent advances on next generation of polyzwitterion-based nano-vectors for targeted drug delivery. *J Control Release*. 2022;343:492–505.
  - Jiang S, Cao Z. Ultralow-fouling, functionalizable, and hydrolyzable zwitterionic materials and their derivatives for biological applications. *Adv Mater*. 2010;22:920–32.

49. Zeng S, Quan X, Zhu H, Sun D, Miao Z, Zhang L, et al. Computer simulations on a pH-responsive anticancer drug delivery system using zwitterion-grafted polyamidoamine dendrimer unimolecular micelles. *Langmuir*. 2021;37:1225–34.
50. Cao Z, Yu Q, Xue H, Cheng G, Jiang S. Nanoparticles for drug delivery prepared from amphiphilic plga zwitterionic block copolymers with sharp contrast in polarity between two blocks. *Angew Chem Int Ed Engl*. 2010;49:3771–6.
51. Ryuji T, Shimizu T, Miyahara R, Asai D, Shimazui R, Yoshikawa T, et al. Blood retention and antigenicity of polycarboxybetaine-modified liposomes. *Int J Pharm*. 2020;586: 119521.
52. Langridge TD, Gemeinhart RA. Toward understanding polymer micelle stability: density ultracentrifugation offers insight into polymer micelle stability in human fluids. *J Control Release*. 2020;319:157–67.
53. Huang S, Yu X, Yang L, Song F, Chen G, Lv Z, et al. The efficacy of nimodipine drug delivery using mPEG-PLA micelles and mPEG-PLA/TPGS mixed micelles. *Eur J Pharm Sci*. 2014;63:187–98.
54. Liang X, Guo C, Ma J, Wang J, Chen S, Liu H. Temperature-dependent aggregation and disaggregation of poly(ethylene oxide)-poly(propylene oxide)-poly(ethylene oxide) block copolymer in aqueous solution. *J Phys Chem B*. 2007;111:13217–20.
55. Cheng C, Qu G, Wei J, Yu T, Ding W. Thermodynamics of micellization of sulfobetaine surfactants in aqueous solution. *J Colloid Interfac Sci*. 2012;15:757–63.
56. Boegh M, Nielsen HM. Mucus as a barrier to drug delivery - understanding and mimicking the barrier properties. *Basic Clin Pharmacol Toxicol*. 2015;116:179–86.
57. Bajka BH, Rigby NM, Cross KL, Macierzanka A, Mackie AR. The influence of small intestinal mucus structure on particle transport ex vivo. *Colloid Surf B Biointerfac*. 2015;135:73–80.
58. Lai SK, Wang YY, Hanes J. Mucus-penetrating nanoparticles for drug and gene delivery to mucosal tissues. *Adv Drug Deliv Rev*. 2009;61:158–71.
59. Zhou Y, Chen Z, Zhao D, Li D, He C, Chen X. A pH-Triggered self-unpacking capsule containing zwitterionic hydrogel-coated MOF nanoparticles for efficient oral exendin-4 delivery. *Adv Mater*. 2021;33:2102044.
60. He B, Lin P, Jia Z, Du W, Qu W, Yuan L, et al. The transport mechanisms of polymer nanoparticles in Caco-2 epithelial cells. *Biomaterials*. 2013;34:6082–98.
61. Fan W, Xiang J, Zhou Z, Tang J, Xie T, Li Z, et al. Mucosal penetrating and cell-binding polyzwitterionic micelles as potent oral nanomedicine for cancer drug delivery. *Adv Mater*. 2022;34:2109189.
62. Montizaan D, Yang K, Reker-Smit C, Salvati A. Comparison of the uptake mechanisms of zwitterionic and negatively charged liposomes by HeLa cells. *Nanomedicine*. 2020;30: 102300.
63. Zou J-J, Wei G, Xiong C, Yu Y, Li S, Hu L, et al. Efficient oral insulin delivery enabled by transferrin-coated acid-resistant metal-organic framework nanoparticles. *Sci Adv*. 2022. <https://doi.org/10.1126/sciadv.abm4677>.
64. Szkudelska K, Szkudelski T. The anti-diabetic potential of betaine. Mechanisms of action in rodent models of type 2 diabetes. *Biomed Pharmacother*. 2022;150: 112946.
65. Wang XX, Edelstein MH, Gafter U, Qiu L, Luo Y, Dobrinskikh E, et al. G protein-coupled bile acid Receptor TGR5 activation inhibits kidney disease in obesity and diabetes. *J Am Soc Nephro*. 2016;27:1362.
66. Glass CK, Olefsky JM. Inflammation and lipid signaling in the etiology of insulin resistance. *Cell Metab*. 2012;15:635–45.
67. Rohm TV, Meier DT, Olefsky JM, Donath MY. Inflammation in obesity, diabetes, and related disorders. *Immunity*. 2022;55:31–55.
68. Chávez-Talavera O, Tailleux A, Lefebvre P, Staels B. Bile acid control of metabolism and inflammation in obesity, type 2 diabetes, dyslipidemia, and nonalcoholic fatty liver disease. *Gastroenterology*. 2017;152:1679–1694.e3.
69. de Aguiar Vallim TQ, Tarling EJ, Edwards PA. Pleiotropic roles of bile acids in metabolism. *Cell Metab*. 2013;17:657–69.
70. Broeders EPM, Nascimento EBM, Havekes B, Brans B, Roumans KHM, Tailleux A, et al. The bile acid chenodeoxycholic acid increases human brown adipose tissue activity. *Cell Metab*. 2015;22:418–26.
71. Harms M, Seale P. Brown and beige fat: development, function and therapeutic potential. *Nat Med*. 2013;19:1252–63.
72. Velazquez-Villegas LA, Perino A, Lemos V, Zietak M, Nomura M, Pols TWH, et al. TGR5 signalling promotes mitochondrial fission and beige remodeling of white adipose tissue. *Nat Commun*. 2018;9:245.
73. Bruening JC, Fenselau H. Integrative neurocircuits that control metabolism and food intake. *Science*. 2023. <https://doi.org/10.1126/science.abl7398>.
74. Xia W, Veeragandham P, Cao Y, Xu Y, Rhyne TE, Qian J, et al. Obesity causes mitochondrial fragmentation and dysfunction in white adipocytes due to RalA activation. *Cell Metab*. 2024;6:273–89.
75. Klein S, Gastaldelli A, Yki-Järvinen H, Scherer PE. Why does obesity cause diabetes? *Cell Metab*. 2022;34:11–20.
76. Lumeng CN, Bodzin JL, Saltiel AR. Obesity induces a phenotypic switch in adipose tissue macrophage polarization. *J Clin Invest*. 2007;117:175–84.
77. Perino A, Pols TWH, Nomura M, Stein S, Pellicciari R, Schoonjans K. TGR5 reduces macrophage migration through mTOR-induced C/EBP $\beta$  differential translation. *J Clin Invest*. 2014;124:5424–36.
78. Wen X, Zhang B, Wu B, Xiao H, Li Z, Li R, et al. Signaling pathways in obesity: mechanisms and therapeutic interventions. *Sig Transduct Target Ther*. 2022;7:1–31.
79. Chavakis T, Alexaki VI, Ferrante AW. Macrophage function in adipose tissue homeostasis and metabolic inflammation. *Nat Immunol*. 2023;24:757–66.
80. Wang Y, Tang B, Long L, Luo P, Xiang W, Li X, et al. Improvement of obesity-associated disorders by a small-molecule drug targeting mitochondria of adipose tissue macrophages. *Nat Commun*. 2021;12:102.
81. Chouchani ET, Kajimura S. Metabolic adaptation and maladaptation in adipose tissue. *Nat Med*. 2019;1:189–200.
82. Winer S, Chan Y, Paltser G, Truong D, Tsui H, Bahrami J, et al. Normalization of obesity-associated insulin resistance through immunotherapy. *Nat Med*. 2009;15:921–9.
83. Li Q, Byun J, Choi J, Park J, Lee J, Oh Y-K. Nanomodulator-mediated restructuring of adipose tissue immune microenvironments for antiobesity treatment. *ACS Nano*. 2024;18:9311–30.
84. Chen Y-S, Liu H-M, Lee T-Y. Ursodeoxycholic acid regulates hepatic energy homeostasis and white adipose tissue macrophages polarization in leptin-deficiency obese Mice. *Cells*. 2019;8:253.
85. Clifford BL, Sedgeman LR, Williams KJ, Morand P, Cheng A, Jarrett KE, et al. FXR activation protects against NAFLD via bile-acid-dependent reductions in lipid absorption. *Cell Metab*. 2021;33:1671–1684.e4.

## Publisher's Note

Springer Nature remains neutral with regard to jurisdictional claims in published maps and institutional affiliations.